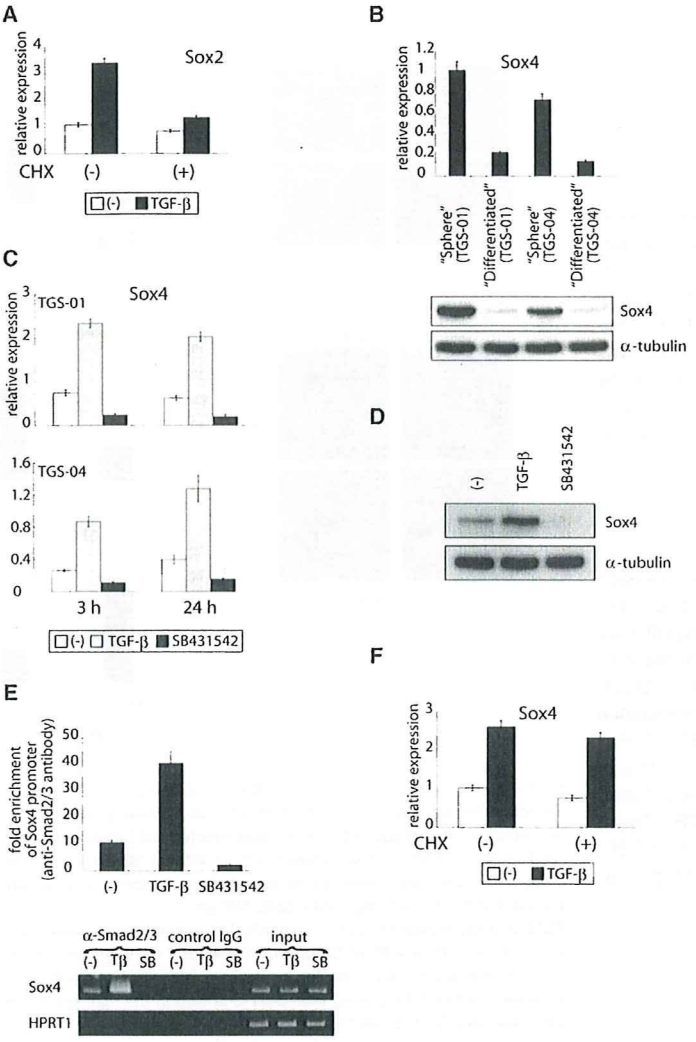

Figure 4. Sox4 Is a Direct Target Gene of TGF-β Signaling

(A) Expression levels of Sox2 mRNA after TGF-β (100 pM) treatment for 24 hr. Treatment with cycloheximide (CHX, 3 μg/ml) was started 30 min before stimulation with TGF-β. Values were normalized to amounts of GAPDH mRNA. Error bars represent SEM.

(B) Expression levels of Sox4 mRNA and protein in "Sphere" cells and "Differentiated" cells. α-tubulin was used as a loading control.

(C) Amount of Sox4 mRNA was determined after TGF-β ligand (100 pM) or inhibitor (SB431542, 1 μM) treatment for 3 or 24 hr. Values were normalized to that of GAPDH mRNA. Error bars represent SEM.

(D) Amount of Sox4 protein was determined after TGF-β ligand (100 pM) or inhibitor (SB431542, 1 μM) treatment for 24 hr. α-tubulin was used as a loading control.

(E) Association of Smad complex with the Sox4 promoter. Chromatin immunoprecipitation analysis was performed using TGS-01 cells treated with TGF-β ligand (100 pM) or inhibitor (SB431542, 1 μM) for 1.5 hr. Eluted DNAs were subjected to quantitative real-time PCR analysis (graph) or conventional RT-PCR (figure). In real-time PCR analysis, values were normalized to the amount of the first intron of hypoxanthine phosphoribosyltransferase (HPRT) 1. Error bars represent SEM. Input, 1%.

(F) Expression levels of Sox4 were analyzed using cDNAs, which were prepared in the experiments shown in (A).

We have shown here that inhibition of TGF-β signaling induces differentiation of glioma-initiating cells and that TGF-β maintains stemness of these cells through induction of Sox2 expression. Moreover, we have demonstrated that Sox4 is a direct target of TGF-β and that Sox4 mediates TGF-β-induced Sox2 expression. Although inhibition of TGF-β signaling markedly promoted differentiation of glioma-initiating cells, addition of TGF-β ligand failed to induce substantial change in glioma-initiating cells. It may be because TGF-β ligand is sufficiently produced by glioma-initiating cells for maintenance of their stemness at the basal level (Figure S5) in spite of the findings that TGF-β signaling itself is not saturated (Figures 2A, 2C, 4C, and 4D). Consistent with these results, overexpression of Sox4 or Sox2 in glioma-initiating cells did not affect their sphere-forming ability in the presence of autocrine TGF-β signaling. These results indicate that in glioma-initiating cells Sox4 and Sox2 are present at sufficient levels for retention of their aggressiveness in the presence of autocrine TGF-β signaling.

Bone morphogenetic protein (BMP) 4, another member of the TGF-β family, promotes differentiation and depletes the pool of glioma-initiating cells (Piccirillo et al., 2006). BMP signaling is known to control the activity of normal brain stem cells (Lim et al., 2000), and TGF-β signaling also regulates normal brain development (Golestaneh and Mishra, 2005; Muñoz-Sanjuán and Brivanlou, 2002). Altogether, the roles of TGF-β and BMP signaling in GSCs may reflect those in normal NSCs, supporting the concept that GSCs and NSCs are closely related (Vescovi et al., 2006).

Sox2 is well known to be one of the self-renewal genes, such as Oct4 and Nanog, and to play pivotal roles in maintaining stemness of embryonic stem cells (Kamachi et al., 2000). Sox2 null mutant embryos cannot give rise to embryonic or trophectoderm lineages (Gubbay et al., 1990). Introduction of Sox2 together with Oct4, Klf4, and c-Myc to human or mouse adult fibroblasts results in generation of induced pluripotent stem (iPS) cells (Takahashi and Yamanaka, 2006; Takahashi et al., 2007). Sox2 also plays essential roles in maintenance of NSCs (Graham et al., 2003), and Sox2 deficiency causes impaired neurogenesis in adult mouse brain (Ferri et al., 2004). Although it was reported that glioma tissues highly express Sox2 mRNA compared to nonmalignant tissues (Ben-Porath et al., 2008; Schmitz et al., 2007), the role of Sox2 in the development of glioma has not yet been determined. In glioma cells, expression levels of Sox2 are linearly and exponentially correlated with those of Nestin and CD133, respectively (Figure S11A, data set from Lee et al., 2006). Here, we demonstrated that knockdown of Sox2 resulted in deprivation of tumorigenic activity of glioma-initiating cells. Our report is the first to show significance of Sox2 in development of glioma and maintenance of the aggressive characters of glioma cells. The results that Sox2 is an essential factor for

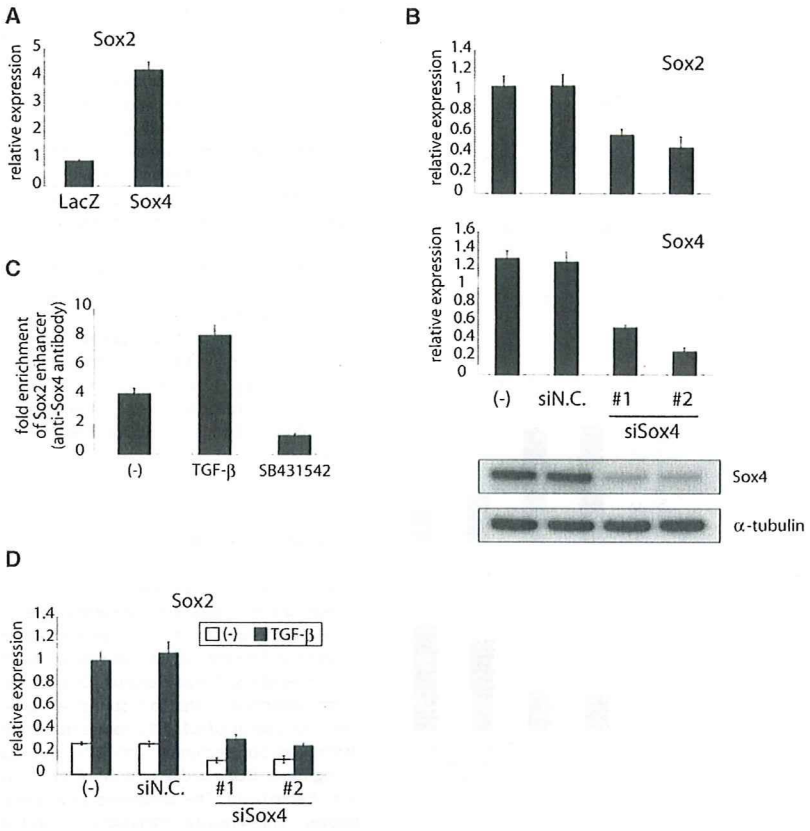

Figure 5. Sox4 Is a Crucial Mediator for TGF-β-Induced Sox2 Expression

(A) Effects of Sox4 overexpression on expression of Sox2. TGS-01 cells were infected with adenovirus-Sox4 or LacZ 24 hr before harvest. Values were normalized to the amount of GAPDH mRNA. Error bars represent SEM.

(B) Effects of Sox4 knockdown on expression of Sox2. Upper graphs show mRNA levels of Sox2 and Sox4. RNA levels were normalized to amounts of GAPDH mRNA. Error bars represent SEM. Lower panels show protein levels of Sox4 and α-tubulin.

(C) Association of Sox4 with the Sox2 enhancer. Chromatin immunoprecipitation analysis was performed using TGS-01 cells treated with TGF-β ligand (100 pM) or inhibitor (SB431542, 1 μM) for 24 hr. Eluted DNAs were subjected to quantitative real-time PCR analysis. Values were normalized to the amount of the first intron of HPRT1. Error bars represent SEM.

(D) TGF-β-induced Sox2 expression under the condition of Sox4 knockdown. Expression levels of Sox2 mRNA after TGF-β (100 pM) treatment for 24 hr were determined by real-time PCR. Indicated siRNAs were transfected 24 hr before TGF-β treatment.

maintenance of GSCs as well as NSCs and embryonic stem cells support the concept that malignant cancer cells and normal developing cells are closely associated with each other in their biological properties. Because Sox2 is a crucial factor for maintenance of other tissue stem cells, it can be speculated that Sox2 also plays significant roles in maintenance of other CSCs.

Although Sox2 is already known to play crucial roles to maintain stemness of NSCs, Sox4 has not been reported to have any function in stem cell properties. So far, Sox4 was reported to be overexpressed in glioma tissues compared to normal brain tissues (Tso et al., 2006), but its role in the development of glioma has not been determined. Here, we have demonstrated that Sox4 binds to Sox2 enhancer region and plays important roles in sustaining tumorigenicity of glioma-initiating cells. From the public data sets, we found that glioma-initiating cells show higher expression of Sox2 and Sox4 and that their expression levels significantly correlate with each other (Figures S11B and S11C, data set from Lee et al., 2006), suggesting that the TGF-β-Sox4-Sox2 pathway is widely used in glioma-initiating cells for retention of their stemness. These findings may add a new player, Sox4, to the concept of stemness.

Sox4 contains a DNA-binding domain known as the HMG box and has been shown to be a transcriptional activator involved in the development of the cardiac outflow tract and the central nervous system (Cheung et al., 2000). So far, Sox4 overexpression has been found to be associated with several human cancer types, including not only glioma but also hepatic cellular carcinoma, prostate cancer, lung cancer, bladder carcinoma, and medulloblastoma (Aaboe et al., 2006; Lee et al., 2002; Liao et al., 2008; Liu et al., 2006b; Pramoonjago et al., 2006; Yokota et al., 2004). The mechanism of Sox4 function as an oncogene, however, has not been fully investigated. From our report, Sox4 can be defined as an oncogene with new mechanisms, at least in glioblastoma.

Although we demonstrated that the TGF-β-Sox4-Sox2 pathway is indispensable for the maintenance of stemness of glioma-initiating cells, the possibility cannot be excluded that other signaling pathways are also involved in it. Hedgehog signaling has been implicated in the development of glioma for many years. It was reported that Hedgehog-Gli1 pathway regulates the stemness of glioma-initiating cells and that cyclopamine, a hedgehog inhibitor, could reduce glioma tumor volume (Clement et al., 2007), though the mechanisms by which inhibition of Hedgehog-Gli1 pathway promotes differentiation of glioma-initiating cells were not investigated. Cyclopamine abrogated sphere-forming ability of TGS-01 cells, but this effect was weaker than that of SB431542, and these two agents failed to show additive or synergistic effects (Figure S12). Therefore, it is likely that there are at least two types of GSCs, Hedgehog-Gli1 pathway-dependent cells and TGF-β-Sox4-Sox2 pathway-dependent cells. To apply Hedgehog inhibitor and TGF-β inhibitor to clinical stages, it will be necessary to assess GSCs of each patient for their signal dependency.

While this manuscript was under revision, Peñuelas et al. (2009) independently reported that TGF-β increases glioma-initiating cell self-renewal through induction of LIF in human glioblastoma. Their results agree with our report in terms of the role

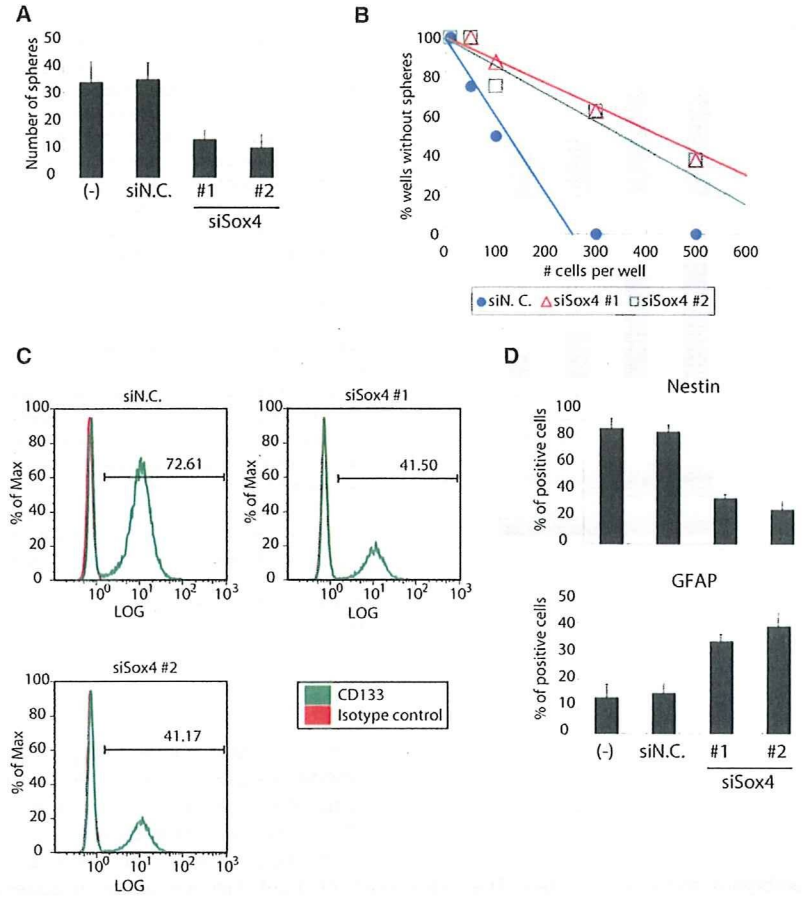

Figure 6. Sox4 Plays Important Roles in Maintenance of Stemness of Glioma-Initiating Cells

(A) TGS-01 cells were dissociated into single-cell populations, transfected with control or Sox4 siRNA duplex, and cultured for 7 days. The data are presented as the number of glioma spheres formed (means ± SEM of five fields).

(B) Knockdown of Sox4 expression by siRNA in TGS-01 cells resulted in a decrease of self-renewal capacity in limiting dilution assay.

(C) Effects of Sox4 knockdown on $CD133^+$ subpopulation of TGS-01 cells were determined by flow cytometry.

(D) Quantification of Nestin-positive or GFAP-positive cells among total cells. Differentiation of TGS-01 cells by Sox4 knockdown was analyzed 7 days after transfection of control (N.C.) or Sox4 siRNA duplex. Error bars represent SEM.

of TGF-β signaling in maintenance of glioma-initiating cells. Although glioma-initiating cells used in our study, TGS-01 and -04, were deprived of their tumorigenicity in the presence of anti-LIF neutralizing antibody (Figure S13), TGF-β signaling failed to induce LIF expression (Figure S7). Taken together, TGF-β signaling may maintain tumorigenicity of glioma-initiating cells through multiple (at least two) independent pathways.

To target TGF-β signaling in glioma, clinical studies of a TGF-β2-specific antisense oligonucleotide AP 12009 in recurrent or refractory high-grade glioma are ongoing (Schlingensiepen et al., 2006). Our findings indicate that such TGF-β inhibitors should be delivered to GSCs, not only to the tumor bulk. This indication will thus pursue the realization of new therapeutic strategies, inducing differentiation of GSCs in addition to suppressing bulk tumor growth. Classical pharmacological therapies cannot sufficiently eradicate GSCs (Liu et al., 2006a). Moreover, GSCs were known to be resistant against radiotherapy (Bao et al., 2006). Our results raise the possibility that TGF-β inhibitors can be used in a combination therapy with classical pharmacological therapies and radiation to make glioblastoma less aggressive. To achieve this, we need to develop a method for delivery of TGF-β inhibitor to GSCs. Delivery of TGF-β inhibitor to GSCs without affecting the functions of normal brain tissues may improve prognosis of GBM, one of the most lethal malignant tumors.

EXPERIMENTAL PROCEDURES

Cell Culture and Reagents

Primary grade IV glioblastoma samples were obtained during surgery from consenting patients, as approved by the Institutional Review Board at the University of Tokyo Hospital (Characteristics of the patients are listed in Figure S1A). Spheres were cultured in DMEM/F12 serum-free medium (Invitrogen) supplemented with B27 (Invitrogen), 20 ng/ml of EGF, and 20 ng/ml of bFGF (both from PeproTech). The antibodies used were as follows: anti-Musashi (Chemicon), anti-Nestin (Chemicon), anti-GFAP (Dako), anti-Tuj1 (Covance), anti-Sox2 (R&D), anti-Sox4 (Santa Cruz), anti-α-tubulin (Sigma-Aldrich), anti-phospho-Smad2 (Zymed Laboratories), anti-Smad2/3 (BD Transduction Laboratories), and phycoerythrin-conjugated CD133/2 (293C3) antibody (Miltenyi Biotec). SB431542 and cycloheximide were purchased from Sigma-Aldrich. Recombinant human TGF-β RII/Fc chimera was from R&D Systems.

Immunostaining

Glioma-initiating cells were seeded on poly-L-ornithine (Sigma)- and fibronectin (Sigma)-coated slide glasses and cultured for 7 days with indicated ligands or inhibitors in serum-free medium. Cells were fixed with 3.7% paraformaldehyde, permealized with PBS containing 0.3% Triton X-100, and incubated with indicated antibodies. Subsequently, samples were incubated with secondary antibodies and stained with propidium iodide (Molecular Probes) for nuclear staining. Stained cells were observed with a confocal microscope (LSM510, Carl Zeiss).

Flow Cytometry

Cells were dissociated into single-cell populations and labeled with a phycoerythrin-conjugated CD133 antibody. The expression level was analyzed using a Beckman Coulter EPICS XL flow cytometer with EXPO32 ADC software.

Sphere-Forming Assay

Glioma-initiating cells were cultured in non-tissue-culture-treated flask (BD Biosciences) with vented caps (BD Biosciences) for 7 days. Floated spheres in five fields per each sample were counted under a microscope (magnification, ×40).

RNA Interference

Small interfering RNAs (siRNAs, see Table S1 for sequences) were purchased from Invitrogen and introduced into cells using Oligofectamine transfection reagent (Invitrogen) according to the manufacturer's instructions.

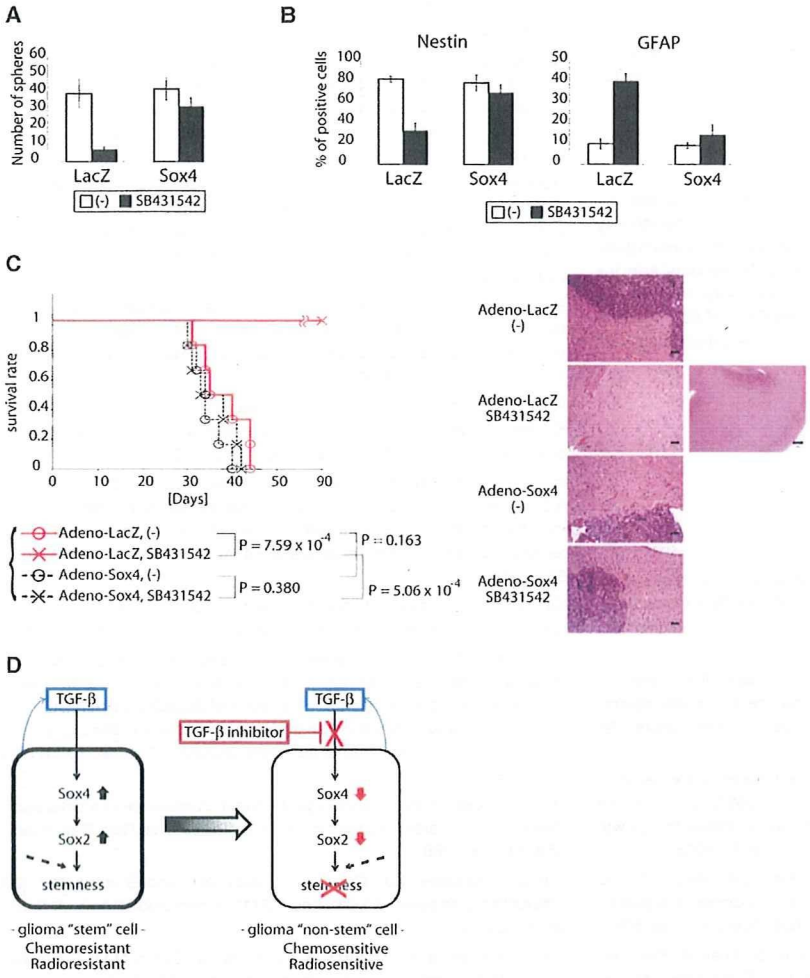

Figure 7. Direct Suppression of Sox4 Expression by TGF-β Inhibitor Is a Critical Step for Differentiation of Glioma-Initiating Cells In Vitro and In Vivo

(A) TGS-01 cells were dissociated into single-cell populations, infected with adenovirus-Sox4 or LacZ, and cultured with or without SB431542 (1 μM) for 7 days. The data are presented as the number of glioma spheres formed (means ± SEM of five fields).

(B) Marker expression of TGS-01 cells infected with adenovirus-Sox4 or LacZ and cultured with or without SB431542 (1 μM) for 7 days. Quantification of Nestin-positive or GFAP-positive cells among total cells is shown in graphs. Error bars represent SEM.

(C) Development of gliomas after intracranial transplantation of 5 × 10^4 TGS-01 cells infected with adenovirus-Sox4 or LacZ (negative control) and treated with or without TGF-β inhibitor (SB431542, 1 μM) for 24 hr. Survival of mice (n = 6 mice for each condition) was evaluated by Kaplan-Meier analysis (left graph). p value was calculated using a log-rank test. Right panels show the results of histological examination of the samples dissected at 30 days after intracranial transplantation. Tissue sections were stained with hematoxylin and eosin. Scale bars, 50 μm in the four left images (×20) or 300 μm in the right image (×4).

(D) Model of maintenance of stemness of glioma-initiating cells by autocrine TGF-β signaling. TGF-β directly induces Sox4 expression. Subsequently, Sox4 promotes expression of Sox2, which plays significant roles in sustaining stemness of glioma-initiating cells, possibly in cooperation with other signaling pathways (dotted arrows). TGF-β inhibitor blocks this "TGF-β-Sox4-Sox2" pathway, promotes differentiation of glioma-initiating cells, and deprives them of aggressiveness.

Adenoviruses

Flag-tagged full-length Sox2 and Sox4 cDNAs were cloned into a pENTR vector (Invitrogen) and introduced into the adenoviral genome via recombination between pENTR vector and the pAd/CMV/V5-DEST vector using LR Clonase (Invitrogen). HEK293A cells were infected with pAd/CMV/Sox2 or pAd/CMV/Sox4 after linearization of it with *PacI*. Viral particles were isolated by three freeze-thaw cycles and amplified by reinfection to HEK293A cells.

Cell Lysis and Immunoblotting

Cells were lysed with a buffer containing 1% Nonidet P-40, 20 mM Tris-HCl (pH 7.4), 150 mM NaCl, 1 mM PMSF, 1% aprotinin, and 5 mM EDTA. Proteins in cleared cell lysates were subjected to SDS-PAGE and transferred to Fluoro Trans W membrane (Pall). Immunoblotting was performed using the indicated antibodies.

Quantitative Real-Time PCR

Quantitative real-time reverse transcription PCR was performed as described previously (Ikushima et al., 2008). All samples were run in triplicate in each experiment. The primers used are listed in Table S1. Values were normalized to that for glyceraldehyde-3-phosphate dehydrogenase (GAPDH).

Limiting Dilution Assay

Sphere cells were dissociated and plated in 96-well plates in 200 μl serum-free medium. After a 7 day culture, the percentage of wells not containing spheres for each cell-plating density was calculated and plotted against the number of cells per well.

Chromatin Immunoprecipitation

Chromatin immunoprecipitation was performed as described previously (Koinuma et al., 2009). Following reverse crosslinking, DNA was treated with proteinase K and purified using a PCR purification kit (QIAGEN). DNA was eluted in 30 μl of TE and used for PCR analysis or quantitative real-time PCR. PCR primers are listed in Table S1.

Intracranial Proliferation Assay

Viable glioma-initiating cells (5 × 10^4) in 5 μl of DMEM/F12 medium were injected stereotactically into the right cerebral hemisphere of 5-week-old female BALB/c *nu/nu* mice at a depth of 3 mm. All animal experimental protocols were performed in accordance with the policies of the Animal Ethics Committee of the University of Tokyo.

Statistical Analysis of Microarray Data

Microarray data were obtained from GEO (http://www.ncbi.nlm.nih.gov/geo/) and ArrayExpress (http://www.ebi.ac.uk/microarray/). Data were analyzed with statistical software R (http://www.R-project.org).

SUPPLEMENTAL DATA

Supplemental Data include one table and 13 figures and can be found with this article online at http://www.cell.com/cell-stem-cell/supplemental/S1934-5909(09)00402-0.

ACKNOWLEDGMENTS

We are grateful to Yasuyuki Morishita, Daisuke Itoh, Hiroshi Yoshida, and Chihana Fujita for skilled technical assistance. This work was supported by KAKENHI (Grant-in-aid for Scientific Research) and Global COE Program (Integrative Life Science Based on the Study of Biosignaling Mechanisms) from the Ministry of Education, Culture, Sports, Science, and Technology of Japan. H.I. has been supported by a Tetsumon-scholarship for the Ph.D.-M.D. program of the University of Tokyo and by a research fellowship of the Japan Society for the Promotion of Science for Young Scientists.

Received: March 12, 2009
Revised: June 17, 2009
Accepted: August 10, 2009
Published: November 5, 2009

REFERENCES

Aaboe, M., Birkenkamp-Demtroder, K., Wiuf, C., Sørensen, F.B., Thykjaer, T., Sauter, G., Jensen, K.M., Dyrskjøt, L., and Ørntoft, T. (2006). SOX4 expression in bladder carcinoma: clinical aspects and in vitro functional characterization. Cancer Res. *66*, 3434–3442.

Bao, S., Wu, Q., McLendon, R.E., Hao, Y., Shi, Q., Hjelmeland, A.B., Dewhirst, M.W., Bigner, D.D., and Rich, J.N. (2006). Glioma stem cells promote radioresistance by preferential activation of the DNA damage response. Nature *444*, 756–760.

Beier, D., Hau, P., Proescholdt, M., Lohmeier, A., Wischhusen, J., Oefner, P.J., Aigner, L., Brawanski, A., Bogdahn, U., and Beier, C.P. (2007). CD133(+) and CD133(-) glioblastoma-derived cancer stem cells show differential growth characteristics and molecular profiles. Cancer Res. *67*, 4010–4015.

Ben-Porath, I., Thomson, M.W., Carey, V.J., Ge, R., Bell, G.W., Regev, A., and Weinberg, R.A. (2008). An embryonic stem cell-like gene expression signature in poorly differentiated aggressive human tumors. Nat. Genet. *40*, 499–507.

Bruna, A., Darken, R.S., Rojo, F., Ocaña, A., Peñuelas, S., Arias, A., Paris, R., Tortosa, A., Mora, J., Baselga, J., et al. (2007). High TGFbeta-Smad activity confers poor prognosis in glioma patients and promotes cell proliferation depending on the methylation of the PDGF-B gene. Cancer Cell *11*, 147–160.

Cheung, M., Abu-Elmagd, M., Clevers, H., and Scotting, P.J. (2000). Roles of Sox4 in central nervous system development. Brain Res. Mol. Brain Res. *79*, 180–191.

Chew, J.L., Loh, Y.H., Zhang, W., Chen, X., Tam, W.L., Yeap, L.S., Li, P., Ang, Y.S., Lim, B., Robson, P., et al. (2005). Reciprocal transcriptional regulation of Pou5f1 and Sox2 via the Oct4/Sox2 complex in embryonic stem cells. Mol. Cell. Biol. *25*, 6031–6046.

Clement, V., Sanchez, P., de Tribolet, N., Radovanovic, I., and Ruiz i Altaba, A. (2007). HEDGEHOG-GLI1 signaling regulates human glioma growth, cancer stem cell self-renewal, and tumorigenicity. Curr. Biol. *17*, 165–172.

Derynck, R., and Zhang, Y.E. (2003). Smad-dependent and Smad-independent pathways in TGF-beta family signalling. Nature *425*, 577–584.

Ehata, S., Hanyu, A., Hayashi, M., Aburatani, H., Kato, Y., Fujime, M., Saitoh, M., Miyazawa, K., Imamura, T., and Miyazono, K. (2007). Transforming growth factor-beta promotes survival of mammary carcinoma cells through induction of antiapoptotic transcription factor DEC1. Cancer Res. *67*, 9694–9703.

Ferri, A.L., Cavallaro, M., Braida, D., Di Cristofano, A., Canta, A., Vezzani, A., Ottolenghi, S., Pandolfi, P.P., Sala, M., DeBiasi, S., et al. (2004). Sox2 deficiency causes neurodegeneration and impaired neurogenesis in the adult mouse brain. Development *131*, 3805–3819.

Golestaneh, N., and Mishra, B. (2005). TGF-beta, neuronal stem cells and glioblastoma. Oncogene *24*, 5722–5730.

Graham, V., Khudyakov, J., Ellis, P., and Pevny, L. (2003). SOX2 functions to maintain neural progenitor identity. Neuron *39*, 749–765.

Gubbay, J., Collignon, J., Koopman, P., Capel, B., Economou, A., Münsterberg, A., Vivian, N., Goodfellow, P., and Lovell-Badge, R. (1990). A gene mapping to the sex-determining region of the mouse Y chromosome is a member of a novel family of embryonically expressed genes. Nature *346*, 245–250.

Günther, H.S., Schmidt, N.O., Phillips, H.S., Kemming, D., Kharbanda, S., Soriano, R., Modrusan, Z., Meissner, H., Westphal, M., and Lamszus, K. (2008). Glioblastoma-derived stem cell-enriched cultures form distinct subgroups according to molecular and phenotypic criteria. Oncogene *27*, 2897–2909.

Hirschmann-Jax, C., Foster, A.E., Wulf, G.G., Nuchtern, J.G., Jax, T.W., Gobel, U., Goodell, M.A., and Brenner, M.K. (2004). A distinct "side population" of cells with high drug efflux capacity in human tumor cells. Proc. Natl. Acad. Sci. USA *101*, 14228–14233.

Ikushima, H., Komuro, A., Isogaya, K., Shinozaki, M., Hellman, U., Miyazawa, K., and Miyazono, K. (2008). An Id-like molecule, HHM, is a synexpression group-restricted regulator of TGF-β signalling. EMBO J. *27*, 2955–2965.

Inman, G.J., Nicolás, F.J., Callahan, J.F., Harling, J.D., Gaster, L.M., Reith, A.D., Laping, N.J., and Hill, C.S. (2002). SB-431542 is a potent and specific inhibitor of transforming growth factor-beta superfamily type I activin receptor-like kinase (ALK) receptors ALK4, ALK5, and ALK7. Mol. Pharmacol. *62*, 65–74.

Kamachi, Y., Uchikawa, M., and Kondoh, H. (2000). Pairing SOX off: with partners in the regulation of embryonic development. Trends Genet. *16*, 182–187.

Koinuma, D., Tsutsumi, S., Kamimura, N., Taniguchi, H., Miyazawa, K., Sunamura, M., Imamura, T., Miyazono, K., and Aburatani, H. (2009). Chromatin immunoprecipitation on microarray analysis of Smad2/3 binding sites reveals roles of ETS1 and TFAP2A in transforming growth factor beta signaling. Mol. Cell. Biol. *29*, 172–186. Published online October 27, 2008. 10.1128/MCB.01038-08.

Kondo, T., Setoguchi, T., and Taga, T. (2004). Persistence of a small subpopulation of cancer stem-like cells in the C6 glioma cell line. Proc. Natl. Acad. Sci. USA *101*, 781–786.

Lee, C.J., Appleby, V.J., Orme, A.T., Chan, W.I., and Scotting, P.J. (2002). Differential expression of SOX4 and SOX11 in medulloblastoma. J. Neurooncol. *57*, 201–214.

Lee, J., Kotliarova, S., Kotliarov, Y., Li, A., Su, Q., Donin, N.M., Pastorino, S., Purow, B.W., Christopher, N., Zhang, W., et al. (2006). Tumor stem cells derived from glioblastomas cultured in bFGF and EGF more closely mirror the phenotype and genotype of primary tumors than do serum-cultured cell lines. Cancer Cell *9*, 391–403.

Liao, Y.L., Sun, Y.M., Chau, G.Y., Chau, Y.P., Lai, T.C., Wang, J.L., Horng, J.T., Hsiao, M., and Tsou, A.P. (2008). Identification of SOX4 target genes using phylogenetic footprinting-based prediction from expression microarrays suggests that overexpression of SOX4 potentiates metastasis in hepatocellular carcinoma. Oncogene *27*, 5578–5589.

Lim, D.A., Tramontin, A.D., Trevejo, J.M., Herrera, D.G., García-Verdugo, J.M., and Alvarez-Buylla, A. (2000). Noggin antagonizes BMP signaling to create a niche for adult neurogenesis. Neuron *28*, 713–726.

Liu, G., Yuan, X., Zeng, Z., Tunici, P., Ng, H., Abdulkadir, I.R., Lu, L., Irvin, D., Black, K.L., and Yu, J.S. (2006a). Analysis of gene expression and chemoresistance of CD133+ cancer stem cells in glioblastoma. Mol. Cancer *5*, 67.

Liu, P., Ramachandran, S., Ali Seyed, M., Scharer, C.D., Laycock, N., Dalton, W.B., Williams, H., Karanam, S., Datta, M.W., Jaye, D.L., et al. (2006b). Sex-determining region Y box 4 is a transforming oncogene in human prostate cancer cells. Cancer Res. *66*, 4011–4019.

Mani, S.A., Guo, W., Liao, M.J., Eaton, E.N., Ayyanan, A., Zhou, A.Y., Brooks, M., Reinhard, F., Zhang, C.C., Shipitsin, M., et al. (2008). The epithelial-mesenchymal transition generates cells with properties of stem cells. Cell *133*, 704–715.

Massagué, J. (2008). TGFbeta in cancer. Cell *134*, 215–230.

Matsuyama, S., Iwadate, M., Kondo, M., Saitoh, M., Hanyu, A., Shimizu, K., Aburatani, H., Mishima, H.K., Imamura, T., Miyazono, K., et al. (2003). SB-431542 and

Gleevec inhibit transforming growth factor-beta-induced proliferation of human osteosarcoma cells. Cancer Res. *63*, 7791–7798.

Miyazawa, K., Shinozaki, M., Hara, T., Furuya, T., and Miyazono, K. (2002). Two major Smad pathways in TGF-beta superfamily signalling. Genes Cells *7*, 1191–1204.

Muñoz-Sanjuán, I., and Brivanlou, A.H. (2002). Neural induction, the default model and embryonic stem cells. Nat. Rev. Neurosci. *3*, 271–280.

Peñuelas, S., Anido, J., Prieto-Sánchez, R.M., Folch, G., Barba, I., Cuartas, I., García-Dorado, D., Poca, M.A., Sahuquillo, J., Baselga, J., et al. (2009). TGF-beta increases glioma-initiating cell self-renewal through the induction of LIF in human glioblastoma. Cancer Cell *15*, 315–327.

Piccirillo, S.G., Reynolds, B.A., Zanetti, N., Lamorte, G., Binda, E., Broggi, G., Brem, H., Olivi, A., Dimeco, F., and Vescovi, A.L. (2006). Bone morphogenetic proteins inhibit the tumorigenic potential of human brain tumour-initiating cells. Nature *444*, 761–765.

Pramoonjago, P., Baras, A.S., and Moskaluk, C.A. (2006). Knockdown of Sox4 expression by RNAi induces apoptosis in ACC3 cells. Oncogene *25*, 5626–5639.

Sánchez-Capelo, A. (2005). Dual role for TGF-beta1 in apoptosis. Cytokine Growth Factor Rev. *16*, 15–34.

Sawyer, J.S., Anderson, B.D., Beight, D.W., Campbell, R.M., Jones, M.L., Herron, D.K., Lampe, J.W., McCowan, J.R., McMillen, W.T., Mort, N., et al. (2003). Synthesis and activity of new aryl- and heteroaryl-substituted pyrazole inhibitors of the transforming growth factor-beta type I receptor kinase domain. J. Med. Chem. *46*, 3953–3956.

Schlingensiepen, K.H., Schlingensiepen, R., Steinbrecher, A., Hau, P., Bogdahn, U., Fischer-Blass, B., and Jachimczak, P. (2006). Targeted tumor therapy with the TGF-beta2 antisense compound AP 12009. Cytokine Growth Factor Rev. *17*, 129–139.

Schmitz, M., Temme, A., Senner, V., Ebner, R., Schwind, S., Stevanovic, S., Wehner, R., Schackert, G., Schackert, H.K., Fussel, M., et al. (2007). Identification of SOX2 as a novel glioma-associated antigen and potential target for T cell-based immunotherapy. Br. J. Cancer *96*, 1293–1301.

Singh, S.K., Hawkins, C., Clarke, I.D., Squire, J.A., Bayani, J., Hide, T., Henkelman, R.M., Cusimano, M.D., and Dirks, P.B. (2004). Identification of human brain tumour initiating cells. Nature *432*, 396–401.

Surawicz, T.S., Davis, F., Freels, S., Laws, E.R., and Menck, H.R. (1998). Brain tumor survival: results from the National Cancer Data Base. J. Neurooncol. *40*, 151–160.

Takahashi, K., Tanabe, K., Ohnuki, M., Narita, M., Ichisaka, T., Tomoda, K., and Yamanaka, S. (2007). Induction of pluripotent stem cells from adult human fibroblasts by defined factors. Cell *131*, 861–872.

Takahashi, K., and Yamanaka, S. (2006). Induction of pluripotent stem cells from mouse embryonic and adult fibroblast cultures by defined factors. Cell *126*, 663–676.

Tojo, M., Hamashima, Y., Hanyu, A., Kajimoto, T., Saitoh, M., Miyazono, K., Node, M., and Imamura, T. (2005). The ALK-5 inhibitor A-83-01 inhibits Smad signaling and epithelial-to-mesenchymal transition by transforming growth factor-beta. Cancer Sci. *96*, 791–800.

Tomioka, M., Nishimoto, M., Miyagi, S., Katayanagi, T., Fukui, N., Niwa, H., Muramatsu, M., and Okuda, A. (2002). Identification of Sox-2 regulatory region which is under the control of Oct-3/4-Sox-2 complex. Nucleic Acids Res. *30*, 3202–3213.

Tso, C.L., Shintaku, P., Chen, J., Liu, Q., Liu, J., Chen, Z., Yoshimoto, K., Mischel, P.S., Cloughesy, T.F., Liau, L.M., et al. (2006). Primary glioblastomas express mesenchymal stem-like properties. Mol. Cancer Res. *4*, 607–619.

Vescovi, A.L., Galli, R., and Reynolds, B.A. (2006). Brain tumour stem cells. Nat. Rev. Cancer *6*, 425–436.

Xu, R.H., Sampsell-Barron, T.L., Gu, F., Root, S., Peck, R.M., Pan, G., Yu, J., Antosiewicz-Bourget, J., Tian, S., Stewart, R., et al. (2008). NANOG is a direct target of TGFbeta/activin-mediated SMAD signaling in human ESCs. Cell Stem Cell *3*, 196–206.

Yokota, N., Mainprize, T.G., Taylor, M.D., Kohata, T., Loreto, M., Ueda, S., Dura, W., Grajkowska, W., Kuo, J.S., and Rutka, J.T. (2004). Identification of differentially expressed and developmentally regulated genes in medulloblastoma using suppression subtraction hybridization. Oncogene *23*, 3444–3453.

Comparison of the effects of the kinase inhibitors imatinib, sorafenib, and transforming growth factor-β receptor inhibitor on extravasation of nanoparticles from neovasculature

Mitsunobu R. Kano,[1,2,3,4] Yukari Komuta,[1,5] Caname Iwata,[1] Masako Oka,[1] Yo-taro Shirai,[1] Yasuyuki Morishita,[1] Yasuyoshi Ouchi,[4] Kazunori Kataoka[2] and Kohei Miyazono[1,2,6]

[1]Department of Molecular Pathology, Graduate School of Medicine, University of Tokyo, 7-3-1 Hongo, Bunkyo-ku, Tokyo, 113-0033; [2]Center for Nano-Bio Integration, University of Tokyo, Tokyo, 113-8656; [3]Medical Scientist Training Program, Faculty of Medicine, University of Tokyo, Tokyo, 113-0033; [4]Department of Geriatrics, Graduate School of Medicine, University of Tokyo, 7-3-1 Hongo, Bunkyo-ku, Tokyo, 113-0033; [5]Japan Association for the Advancement of Medical Equipment, 3-42-6 Hongo, Bunkyo-ku, Tokyo, 113-0033, Japan

(Received May 20, 2008/Revised September 11, 2008/Accepted September 14, 2008/Online publication November 25, 2008)

There are a number of kinase inhibitors that regulate components of the neovasculature. We previously reported the use of transforming growth factor (TGF)-β inhibitor on neovasculature in stroma-rich tumor models to increase the intratumoral distribution of nanoparticles. Here, we compared the effects of two other kinase inhibitors, imatinib and sorafenib, with TGF-β inhibitor (LY364947) on extravasation of a modeled nanoparticle, 2 MDa dextran. We first used a mouse model of neoangiogenesis, the Matrigel plug assay, to compare neovasculature formed inside of and around Matrigel plugs (intraplug and periplug regions, respectively). Intraplug vasculature was more strongly pericyte covered, whereas periplug vasculature was less covered. In this model, TGF-β inhibitor exhibited the most potent effect on intraplug vasculature in increasing the extravasation of dextran, whereas sorafenib had the strongest effect on periplug vasculature. Although imatinib and TGF-β inhibitor each reduced pericyte coverage, imatinib also reduced the density of endothelium, resulting in a decrease in overall delivery of nanoparticles. These findings were confirmed in two tumor models, the CT26 colon cancer model and the BxPC3 pancreatic cancer model. The vasculature phenotype in the CT26 model resembled that in the periplug region, whereas the latter resembled that in the intraplug region. Consistent with this, sorafenib most potently enhanced the accumulation of nanoparticles in the CT26 model, whereas TGF-β inhibitor did in the BxPC3 model. In conclusion, the appropriate strategy for optimization of tumor vasculature for nanoparticles may differ depending on tumor type, and in particular on the degree of pericyte coverage around the vasculature. (*Cancer Sci* 2009; 100: 173–180)

The effectiveness of drug delivery into tumor tissues is an important issue in the treatment of solid tumors, in addition to the efficacy of drugs in treating tumor cells. For example, gemcitabine, a first-line anticancer agent for pancreatic adenocarcinoma, exhibited potent *in vitro* growth-inhibitory effects on a cultured cell line derived from the human pancreatic adenocarcinoma line BxPC3.[1] However, it exhibited only slight inhibitory effects on xenografted BxPC3 tumors in mice[2] and slight elongation of survival time in tumor-bearing patients, with significant effects only in the improvement of quality of life index in clinical trials.[3]

Many factors might potentially explain this discrepancy, particularly those related to tumor stroma.[4] Among them, tumor vasculature plays an important role in the delivery of anticancer agents. Extravasation of drugs to tumor tissue constitutes an essential part of drug delivery to tumor tissues,[5] whereas the molecular size of compounds is another important determinant of accumulation.[6] We have recently shown that increased leakiness in tumor neovasculature improves the accumulation of nanoparticles in tumor tissues in animal models of pancreatic adenocarcinoma and diffuse-type advanced gastric cancer.[7] In that study, inhibition of transforming growth factor (TGF)-β signaling reduced pericyte coverage and slightly increased endothelial area, resulting in an increase in vascular leakiness without loss of blood flow. However, numerous studies of tumor neovasculature have shown that it is leaky by nature, and that manipulation of vessels to make them less leaky, or induction of vascular normalization, may therefore benefit drug delivery to tumor tissues.[8] This theory has been supported with the use of vascular endothelial growth factor (VEGF) inhibitors. There are a number of VEGF inhibitors available, including neutralizing anti-VEGF antibodies such as bevacizumab (Avastin) and sorafenib (Nexavar). Sorafenib is a small molecular-weight (SMW) compound inhibiting multiple tyrosine kinases, including VEGF receptor (VEGFR) 2.[9]

The roles of pericytes in neoangiogenesis have also been well investigated.[10] Coverage of the neovasculature by pericytes stabilizes vascular structure.[11] Genetic ablation of platelet-derived growth factor (PDGF)-B signaling, one of the major signaling pathways in induction of pericyte maturation and recruitment to the endothelium, results in a bleeding tendency of the neovasculature.[11–13] PDGF-B signaling can be inhibited by the SMW inhibitor (SMWI) imatinib (Gleevec or Glivec), which inhibits the receptor for PDGF-B signaling, PDGF receptor (PDGFR) β, as well as PDGFRα and c-kit.[14] The use of imatinib along with VEGF inhibitors was shown to be effective in inhibiting tumor neovascularization in an animal model of spontaneous pancreatic islet tumor, the RIP-Tag model, through disruption of both pericytes and endothelium.[15]

Here we investigated the changes in vascular leakiness induced by three of the SMWI mentioned above, TGF-β inhibitor (LY364947), sorafenib, and imatinib, in the Matrigel plug assay as well as two animal cancer models. The Matrigel plug assay was carried out by mixing BD Matrigel Basement Membrane Matrix with VEGF-A, fibroblast growth factor (FGF)-2, and

[6]To whom correspondence should be addressed. E-mail: miyazono-ind@umin.ac.jp

doi: 10.1111/j.1349-7006.2008.01003.x

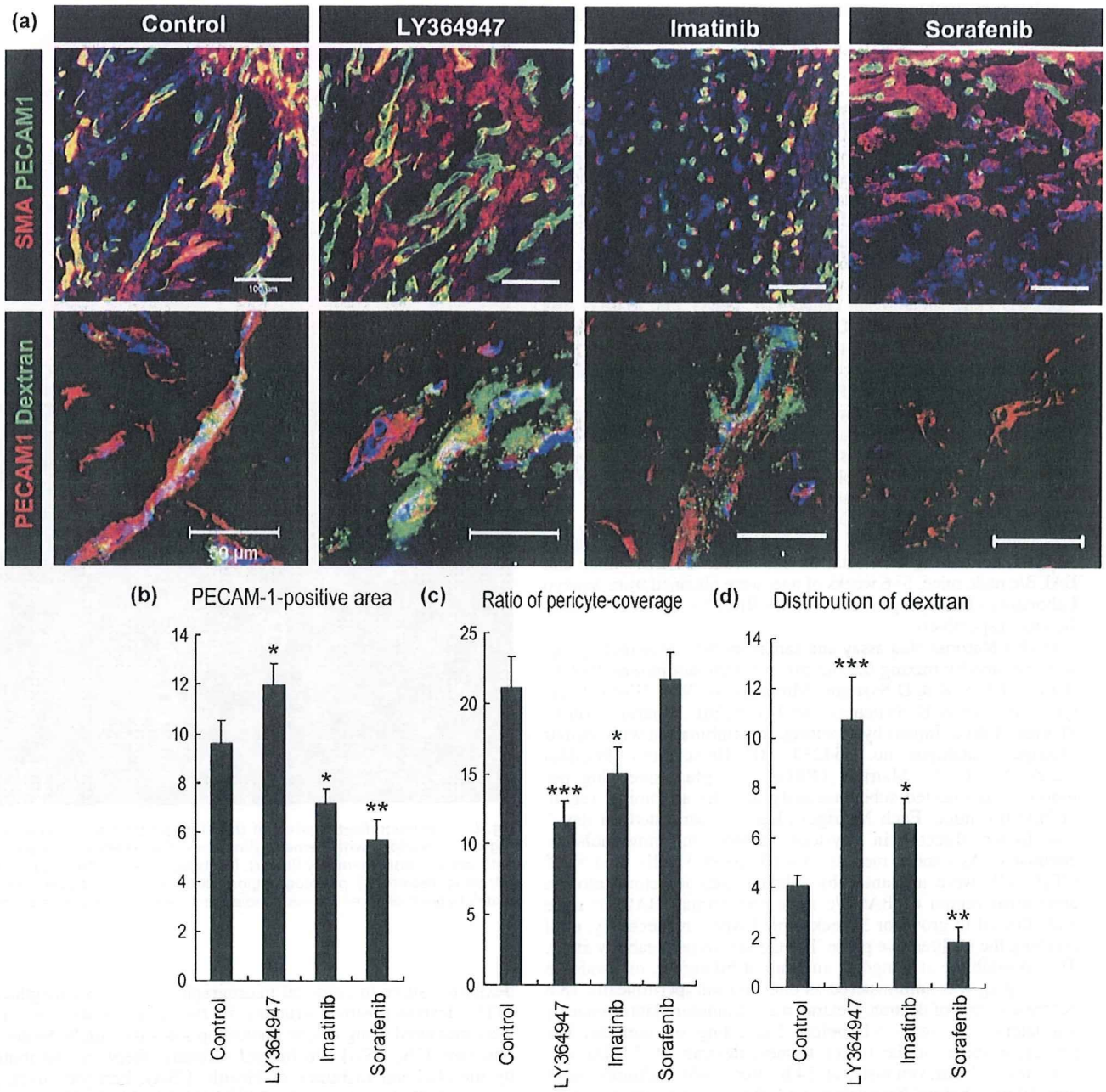

Fig. 1. The effects of three types of kinase inhibitors on extravasation of dextran in the Matrigel plug assay. (a) Confocal microscopy analyses. Upper row: staining of platelet endothelial cell adhesion molecule (PECAM)-1-positive endothelium in green and smooth muscle α-actin (SMA)-positive pericytes in red. Scale bars = 100 μm. Lower row: distribution of 2 MDa dextran in green and PECAM-1-positive endothelium in red. Scale bars = 50 μm. (b–d) Results of quantification (n = 15) of areas of endothelium (b, in percentage in one microscopic view), ratio of pericyte-covered endothelium (c, in percentage), and dextran distribution (d, in percentage in one microscopic view). Bars in the graphs represent standard errors. $^{*}P < 0.05$; $^{**}P < 0.01$; and $^{***}P < 0.001$.

heparin as angiogenic molecules to form mature neovasculature inside the gel plug, according to our previous report.[16] Of the two cancer models used in the present study, one was a well-established hypervascular cancer model using the murine colon cancer cell line CT26, whereas the other was an interstitium-rich cancer model using the human pancreatic cancer cell line BxPC3. With the latter model, we previously demonstrated therapeutic effects of combined use of TGF-β inhibitor on nanoparticles.[7] Using these models, we investigated the effects of SMWI on the distribution of 2 MDa dextran, a model of nanoparticles with an estimated hydrodynamic diameter of 50 nm.[6] The Matrigel plug assay and tumor model experiments revealed that TGF-β inhibitor increased extravasation of 2 MDa dextran in pericyte-covered neovasculature, whereas sorafenib increased that in vasculature with less pericyte coverage. These findings are important for determination of the optimal choice of angiogenic

doi: 10.1111/j.1349-7006.2008.01003.x

regulators in combination with nanoparticles for chemotherapy of cancer in general.

Materials and Methods

Reagents and antibodies. TGF-β inhibitor was purchased from Calbiochem (San Diego, CA, USA; LY364947, catalog no. 616451), imatinib was from Novartis Pharma (Tokyo, Japan), and sorafenib was from Bayer Healthcare (West Haven, CT, USA). These compounds were diluted in dimethyl sulfoxide to 5, 25, and 10 mg/mL, respectively, as stock solutions. Fluorescein isothiocyanate (FITC)-conjugated dextran of 2 000 000 Da (2 MDa) was obtained from Sigma-Aldrich (St Louis, MO, USA). The antibody to platelet endothelial cell adhesion molecule (PECAM)-1 was from BD PharMingen (San Diego, CA, USA), that to NG2 was from Chemicon (Temecula, CA, USA), and that to smooth muscle α-actin (SMA) (Cy3-conjugated) was from Sigma-Aldrich. AlexaFluor-conjugated secondary antibodies were purchased from Invitrogen Molecular Probes (Eugene, OR, USA).

Cancer cell lines and animals. The BxPC3 human pancreatic adenocarcinoma cell line was obtained from the American Type Culture Collection (Manassas, VA, USA), and was grown in RPMI-1640 medium supplemented with 10% fetal bovine serum. The murine colon adenocarcinoma CT26 cell line was from the National Cancer Center Research Institute, Japan, and was cultured in Dulbecco's modified Eagle's medium (Sigma-Aldrich) containing 10% fetal bovine serum. BALB/c mice and BALB/c nude mice, 5–6 weeks of age, were obtained from Sankyo Laboratory (Tokyo, Japan) and Charles River Laboratories (Tokyo, Japan), respectively.

***In vivo* Matrigel plug assay and cancer models.** Matrigel plugs were created by mixing 0.2 mg/mL recombinant human VEGF-A (VEGF165; R & D Systems, Minneapolis, MN, USA), 1 mg/mL FGF-2 (R & D Systems), and 0.1 mg/mL heparin (Aventis Pharma, Tokyo, Japan) by pipetting, in combination with regular Matrigel (catalogue no. 354234; BD Biosciences, Franklin Lakes, NJ, USA). Matrigel (400 μL per plug; one plug per mouse) was injected subcutaneously into the abdominal region of BALB/c mice. Each Matrigel plug was harvested on day 7 and frozen directly in dry-iced acetone for immunohistochemistry. As cancer models, 5×10^6 BxPC3 cells or 1×10^6 CT26 cells were implanted by subcutaneous injection into the abdominal region of BALB/c nude and normal BALB/c mice and allowed to grow for 3 weeks and 1 week, respectively, until reaching the proliferative phase. For the *in vivo* permeability assay, TGF-β inhibitor at 1 mg/kg, imatinib at 50 mg/kg, or sorafenib at 40 mg/kg was administered as one shot intraperitoneally 18 h before injection of dextran. Dextran was administered intravenously via lateral tail veins 6 h before harvesting of samples. For perfusion study in the tumor tissues, dextran of 2 MDa was administered intravenously, at 24 h after SMWI-administration and 10 min before harvesting, and the excised samples were directly fixed in formalin. All experimental protocols were carried out in accordance with the policies of the Animal Ethics Committee at the University of Tokyo.

Histology and immunohistochemistry. The excised samples were either directly frozen in dry-iced acetone for immunohistochemistry, or fixed overnight in 4% paraformaldehyde and then paraffin embedded to prepare them for hematoxylin–eosin (HE) staining or perfusion study in the tumor tissues. Frozen samples were further sectioned at 10 μm thickness in a cryostat, briefly fixed with 10% formalin, and then incubated with primary and fluorescent secondary antibodies. Samples were observed with a LSM510 Meta confocal microscope (Zeiss, Thornwood, NY, USA) for immunohistochemistry, and with an AX80 microscope (Olympus, Tokyo, Japan) for HE staining.

Quantification. Areas in Matrigel plugs that were PECAM-1-positive, double-positive for PECAM-1 and SMA, and FITC–dextran-positive in confocal micrographs ($n = 15$), or lengths of FITC–dextran-positive structure in the tumor tissues ($n = 12$) were measured using Adobe Photoshop software (Adobe Systems, San Jose, CA, USA) and ImageJ software (freeware distributed by the National Institutes of Health, USA). Pericyte coverage was quantified as the ratio of PECAM-1/SMA-double-positive areas to PECAM-1-positive areas, as described previously.[7] Results were further analyzed statistically by Student's *t*-test using Microsoft Excel software (Microsoft, Redmond WA, USA).

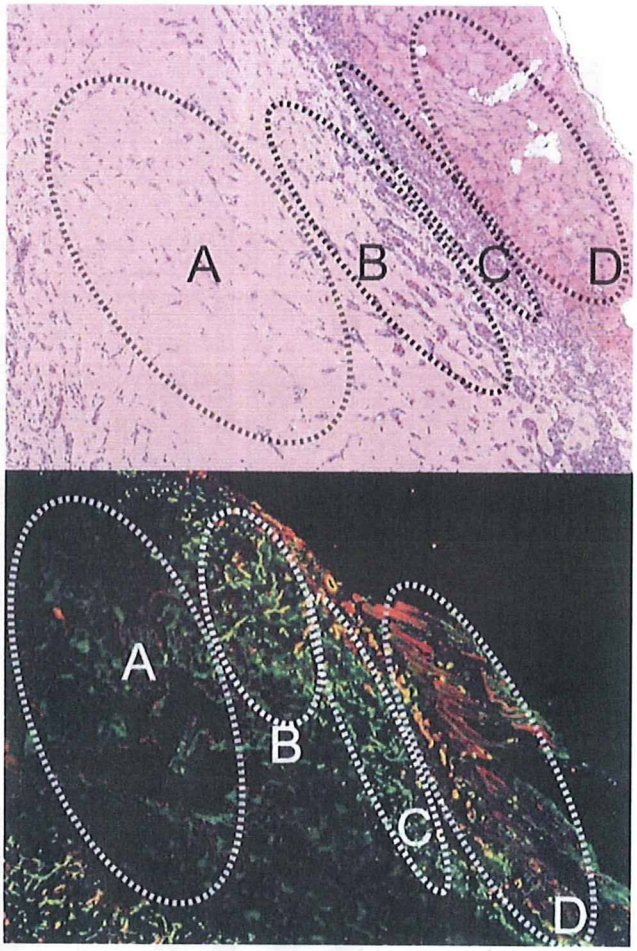

Fig. 2. Low-magnification view of the Matrigel plug and surrounding regions in sections with hematoxyline-eosin (HE) staining (upper) and with immunohistochemistry (lower). (a) Avascular area, (b) vascularized intraplug region, (c) periplug region, and (d) normal tissue. Green, platelet endothelial cell adhesion molecule-1; red, smooth muscle α-actin.

Results

We initially carried out the Matrigel plug assay *in vivo*, in which regular Matrigel was mixed with VEGF-A, FGF-2, and heparin[16] to investigate the effects of three SMWI on the extravasation of 2 MDa dextran (Fig. 1). Marked induction of pericyte-covered mature neovasculature was observed in the gel plug after a 7-day incubation in mice, as we reported previously.[16] Pericytes were determined to be SMA-positive cells in a Matrigel plug assay. In this model, administration of TGF-β inhibitor decreased pericyte coverage of the neovasculature and significantly enhanced the distribution of 2 MDa dextran. This observation was consistent

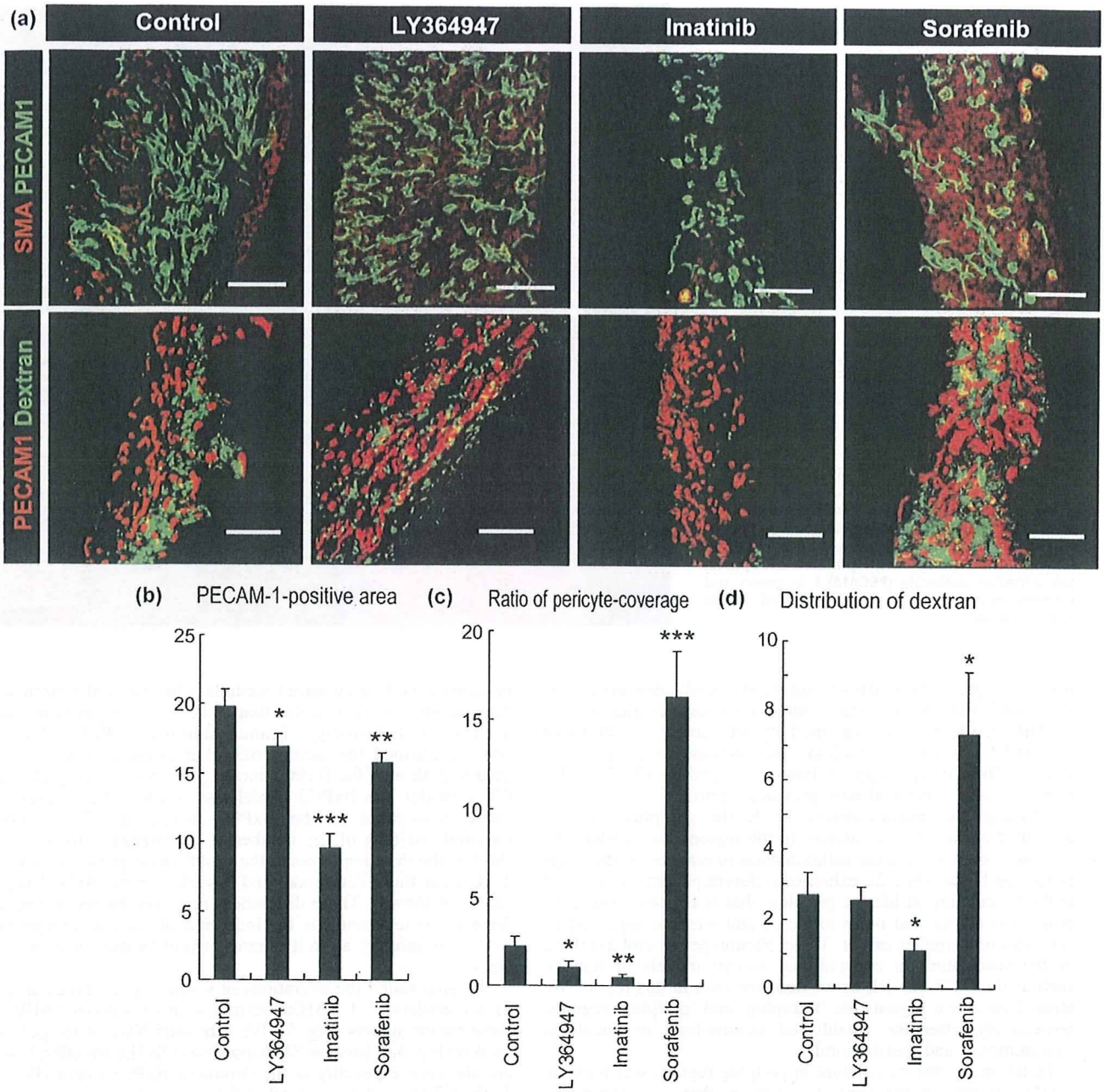

Fig. 3. Effects of three types of kinase inhibitors on extravasation of dextran from vasculature in the periplug region. (a) Confocal microscopy analyses. Upper row: staining of platelet endothelial cell adhesion molecule (PECAM)-1-positive endothelium in green and smooth muscle α-actin (SMA)-positive pericytes in red. Lower row: distribution of 2 MDa dextran in green and PECAM-1-positive endothelium in red. Scale bars = 100 μm. (b–d) Results of quantification (n = 15) of areas of endothelium (b, in percentage in one microscopic view), ratio of pericyte-covered endothelium (c, in percentage), and dextran distribution (d, in percentage in one microscopic view). Bars in the graphs represent standard errors. $^{*}P < 0.05$; $^{**}P < 0.01$; and $^{***}P < 0.001$.

with our previous study, in which we used animal models of pancreatic adenocarcinoma and diffuse-type gastric cancer.[7] Based on this result, we expected that a decrease in pericytes might induce more extravasation of 2 MDa dextran.

To confirm this, we compared the effects of imatinib administration, which inhibits PDGF signaling and may therefore decrease pericyte coverage. However, administration of imatinib decreased the total accumulation of 2 MDa dextran compared with TGF-β inhibitor (Fig. 1). Although imatinib actually decreased pericyte coverage to the same level of TGF-β inhibitor, it also decreased PECAM-1-positive endothelium together with pericyte coverage. These findings of morphological analysis were consistent with those noted in a previous report.[17] TGF-β inhibitor maintained the area of PECAM-1-positive endothelium and may therefore be superior to imatinib. In addition, although VEGF inhibition was expected to increase drug delivery, based on the

doi: 10.1111/j.1349-7006.2008.01003.x

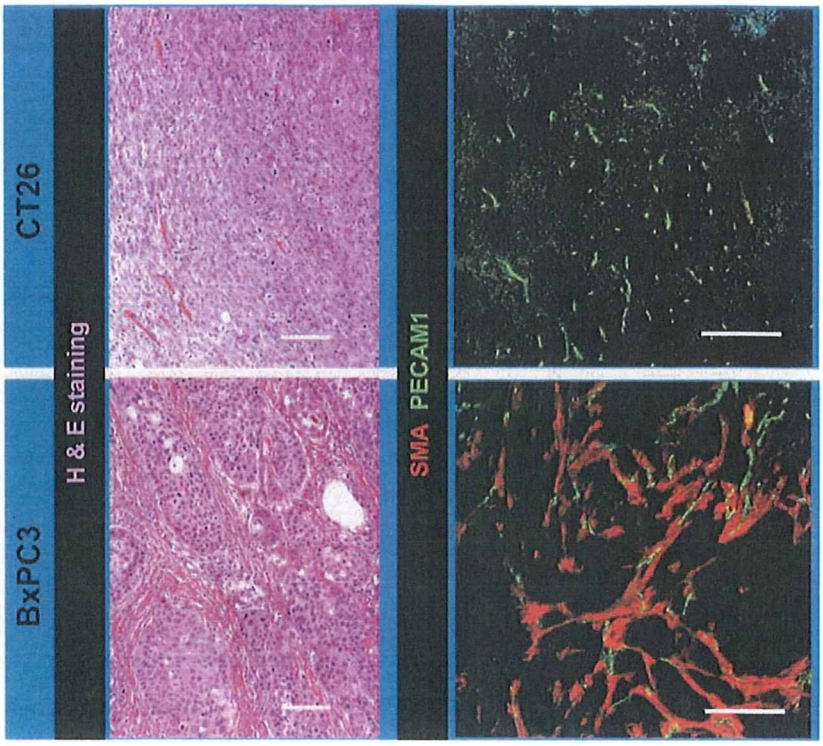

Fig. 4. Two animal tumor models using CT26 and BxPC3 cell lines. Histological examination of tumor models by hematoxylin–eosin staining and immunohistochemistry with platelet endothelial cell adhesion molecule (PECAM)-1 in green and smooth muscle α-actin (SMA) in red. Scale bars = 100 μm.

results of previous studies,[8] sorafenib nearly eliminated the influx of 2 MDa dextran and resulted in far less accumulation of it. This result can be explained by the potent reduction of PECAM-1-positive endothelium and increase in pericytes as sleeves. These morphological changes induced by VEGF inhibition were also consistent with previous reports.[18]

Although the neovasculature inside the gel plugs was as described above, the vasculature in the regions surrounding the gel plugs, or sites of acute inflammation in reaction to the plugs as foreign bodies (Fig. 2), exhibited different patterns. Compared to the vasculature inside the gel plug, that in regions around the plugs was denser and more tortuous, and was accompanied by pericytes to a smaller extent. These phenotypes resembled those of the vasculature in conventional animal models of tumors, such as the CT26 model, as we describe later in this report. We termed these two regions the 'intraplug' and 'periplug' regions, respectively, after the established terminology in oncology, 'intratumoral' and 'peritumoral'.

Functionally, the vasculature in periplug regions was leaky to 2 MDa dextran in the control condition, that is, without any modulation by SMWI (Fig. 3). Surprisingly, the effects of SMWI on neovasculature in the periplug regions were quite different from those in the intraplug regions. In the periplug regions, pericyte coverage of the neovasculature was far less than in the intraplug region, even in the control condition. In this periplug region, neither TGF-β inhibitor nor imatinib significantly altered pericyte coverage. Consequently, these compounds did not alter the accumulation of 2 MDa dextran. Sorafenib, on the other hand, did increase pericyte coverage, and increased the accumulation of 2 MDa dextran. This increase in extravasation was consistent with previous reports on the effects of VEGF inhibition.[8]

We subsequently compared these findings in the Matrigel plug assay with those in two subcutaneous tumor xenograft models. We used the CT26 cell line derived from murine colon cancer and the BxPC3 cell line derived from human pancreatic adenocarcinoma (Fig. 4). HE staining of CT26 xenografts revealed a well-vascularized medullary histological pattern with little tumor stroma, whereas that of BxPC3 xenografts revealed a stroma-rich histology. Immunostaining of PECAM-1 and SMA confirmed this stroma-rich characteristic of the BxPC3 model. Although the BxPC3 model grew more slowly than the CT26 model, the BxPC3 model also reached the proliferative phase. Compared to the BxPC3 model, the CT26 model required one-fifth of the number of inoculating cells and one-third of the duration to reach the proliferative phase, which was 1 week for the CT26 model and 3 weeks for the BxPC3 model (data not shown). These differences may well be due to the differences in requirements for induction of stromal components from host animals, as well as rates of proliferation of tumor cell lines.

We then tested the alterations in vascular phenotypes as well as accumulation of 2 MDa dextran with or without SMWI in these tumor models (Fig. 5). We here used NG2 as the pericyte marker (Fig. 5a), because SMA-positive cells (i.e. myofibroblasts) are abundant especially in the stroma of BxPC3 tumor (Fig. 4). In the CT26 model, sorafenib did increase the pericyte-covered vasculature, whereas other SMWI did not increase the pericytes. Imatinib decreased endothelial cells. These observations in the CT26 tumor model were consistent with those in the periplug region of the Matrigel plug. In the BxPC3 model, pericyte coverage was less with LY364947 and imatinib, and endothelial cells were decreased with imatinib and sorafenib. These findings in the BxPC3 tumor model were consistent with those in the intraplug region. Accordingly, 2 MDa dextran was diffusely distributed in tumor tissue without any treatment in the CT26 model, whereas almost no leakage of dextran was observed in the BxPC3 model (Fig. 5b). Sorafenib exhibited the best effect in the CT26 model, whereas TGF-β inhibitor did in the BxPC3 model. The latter result was consistent with the findings of our previous work using nanoparticles including PEGylated liposomes incorporating doxorubicin (Doxil) of approximately 100 nm in diameter, which exhibited antitumor effects in the BxPC3 model

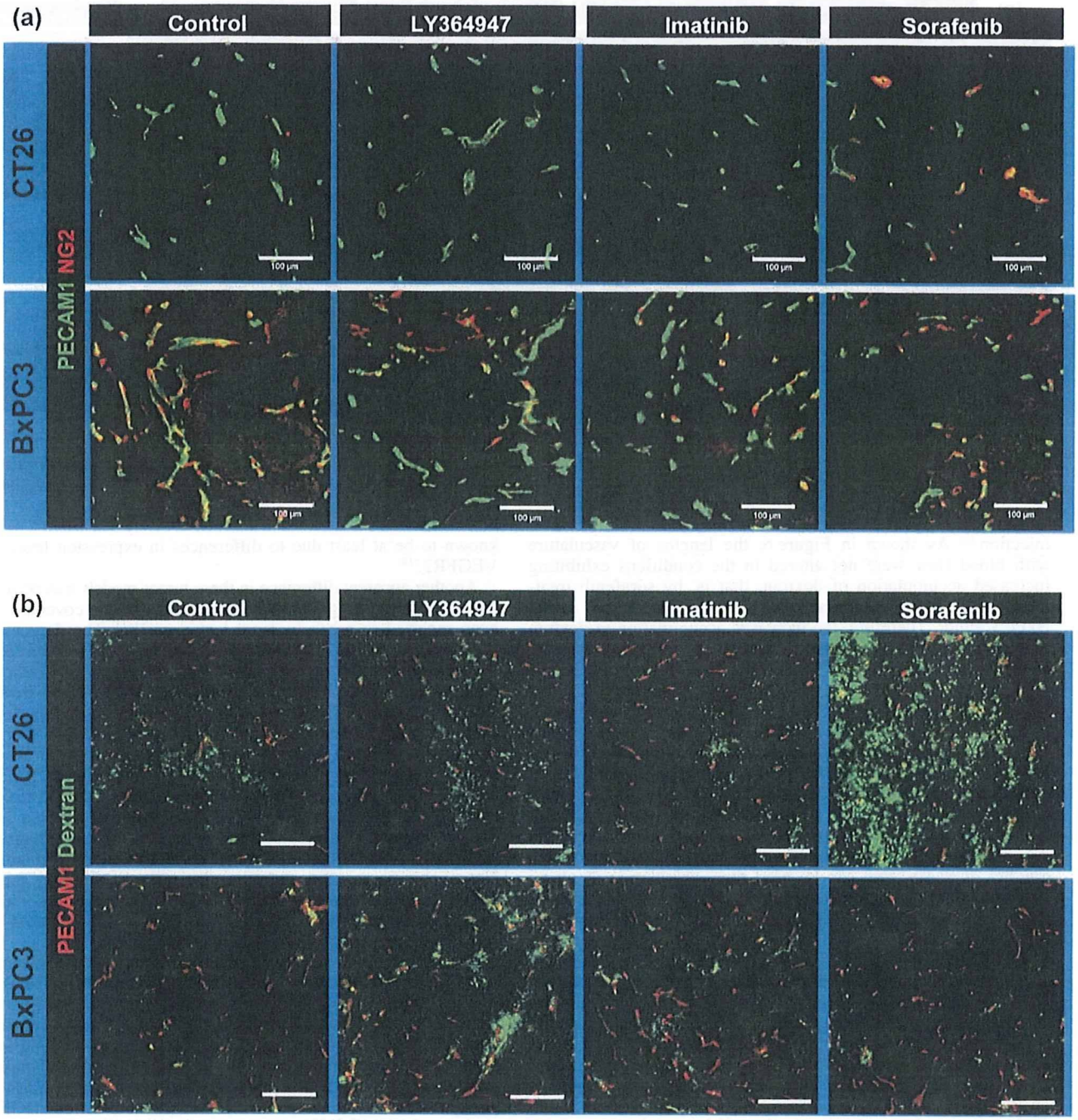

Fig. 5. Effects of three kinase inhibitors in the tumor models. (a) Vascular phenotypes revealed by immunohistochemistry. Green, platelet endothelial cell adhesion molecule (PECAM)-1; red, NG2. (b) Extravasation of 2 MDa dextran from vasculature. Dextran in green and PECAM-1 in red. Scale bars = 100 μm.

only when combined with TGF-β inhibitor.[7] We also tested the effects of Doxil with or without TGF-β inhibitor in the CT26 model. Monotherapy with Doxil at 8 mg/kg almost completely inhibited tumor growth, and combined administration of TGF-β inhibitor did not yield any significant additional effects (data not shown). These findings were consistent with those observed in the Matrigel plug assay. The effects of combined use of imatinib were also consistent with those in the Matrigel plug assay.

Increased accumulation of dextran in these tumor models at 7 h after injection, by sorafenib in the CT26 tumor and by LY364947 in the BxPC3 tumor, can also be explained by an increase in the amount of vasculature with perfusion, not only by an increase in leakage. To test this possibility, we examined changes in perfusion by intravascular existence of dextran at only 10 min after administration, because dextran of 2 MDa should basically remain inside vasculature at that time after

doi: 10.1111/j.1349-7006.2008.01003.x

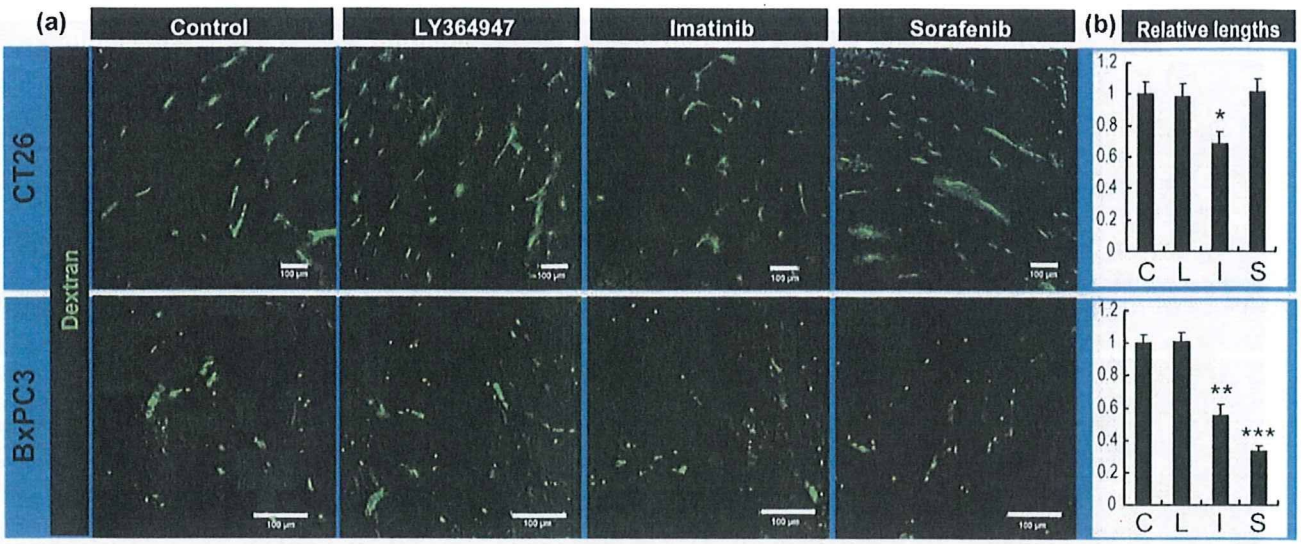

Fig. 6. Perfusion study in the tumor models. (a) Tumor vessels with perfusion were determined by the existence of dextran in green, administrated at 10 min before harvesting. Scale bars = 100 μm. (b) Relative lengths of vessels with perfusion. C, control; I, imatinib; L, LY364947; S, sorafenib. Bars represent standard errors. $*P < 0.05$; $**P < 0.01$; and $***P < 0.001$.

injection.[6] As shown in Figure 6, the lengths of vasculature with blood flow were not altered in the conditions exhibiting increased accumulation of dextran, that is, by sorafenib treatment in the CT26 tumor and by LY364947 treatment in the BxPC3 tumor. Therefore, the increased accumulation of dextran in these conditions may largely be due to an increase in vascular leakiness.

Discussion

We have previously shown that use of short-acting SMW TGF-β inhibitor can increase the distribution of nanoparticles in stroma-rich tumors by increasing the leakiness of the tumor neovasculature.[7] By virtue of the brief duration of SMWI effects, potential side effects can be decreased due to long-term suppression of essential signaling pathways. There are still a number of SMWI that can be used for manipulation of tumor neovasculature via their effects on pericytes or endothelium. We therefore compared the effects of two of these SMWI, imatinib and sorafenib.

Combined use of VEGF inhibition has been reported to have potent effects on drug delivery into tumor tissues.[19] The underlying mechanism for this has been explained by the vascular 'normalization' theory,[8] or decreased interstitial fluid pressure by decreased leakiness of tumor vasculature, via a decrease in endothelial cells and increase in pericyte coverage. Consistent with this, VEGF inhibition by sorafenib had significant effects on the retention of 2 MDa dextran in the periplug regions and in CT26 tumor, where vasculature showed less pericyte coverage and denser endothelium than in normal tissues. However, VEGF inhibition significantly decreased retention of the same dextran in adjacent areas, the intraplug region, and in BxPC3 tumor. Vascular phenotypes in these regions were characterized by more pericyte coverage and sparser endothelium, that is, they were more 'normal' than those in the periplug region and in CT26 tumor.

One of the differences between these two kinds of vasculature was the blood flow in the vasculature after sorafenib treatment. In CT26 tumor after sorafenib treatment, blood flow was maintained, whereas the flow ceased in sorafenib-treated BxPC3 tumor. These differences may partially be because of differences in sensitivity of the endothelium to the change in VEGF signaling, known to be at least due to differences in expression levels of VEGFR2.[18]

Another apparent difference in these tumor models was pericyte coverage before drug administration. Less pericyte coverage has been reported to result in more leakiness.[11–13] The degrees of dextran accumulation in all control conditions (i.e. without modification by SMWI) are consistent with the degrees of pericyte coverage. Increased dextran accumulation in LY364947-treated BxPC3 tumors can also be explained by decreased pericyte coverage, not by normalization. Both blood perfusion (Fig. 6) and interstitial fluid pressure, which we previously reported,[7] did not differ with or without LY364947 treatment in BxPC3 tumor. These findings suggest that we may need different approaches, such as the use of TGF-β inhibitor to increase drug delivery (at least for nanoparticles), to develop effective treatment for tumors with originally 'more normal' tumor vasculature. Note, however, that these more normal vessels in tumors might not be completely normal, because TGF-β inhibitor did not alter the accumulation of nanoparticles in true normal tissues, as we previously reported.[7]

Regarding the degree of original pericyte coverage in tumor vasculature, an increase in the amount of stromal components in tumor tissue may result in an increase in pericyte coverage. In a previous study, we found that the presence of FGF-2 together with VEGF-A enhances mature neovascularization compared with VEGF-A alone.[16] In addition to FGF-2, a set of signaling molecules is needed to recruit and to induce proliferation of pericytes. These include PDGF-BB[12,13] (homodimer of PDGF-B chain) and TGF-β.[11,20] These signaling molecules are reported to be secreted from components of the tumor stroma and, above all, cancer-associated fibro-blasts[21–23] and macrophages.[24] Tumors with more stroma, including fibroblasts and immune cells, have more pericyte coverage of the vasculature with greater maturity and less leakiness. Although chemoresistance of tumors has been largely investigated from the aspect of drug sensitivity of tumor cells per se, it is possible that the histological pattern of the tumor tissues may also constitute a reason for chemoresistance, because of insufficient drug delivery to the tumor cells.

The Tie2–angiopoietin signaling pathway is also known to be involved in vessel maturation and to affect pericytes.[25] Because there are no SMW compounds available to inhibit this signaling pathway, we tested the effects of one-shot Tie2-Fc chimeric

protein at 50 mg/kg bodyweight with 2 MDa dextran in the Matrigel plug assay, but no significant effects on accumulation of 2 MDa dextran were observed (M.R. Kano, unpublished data, 2008). There are two possible explanations for this observation: spatial and temporal. According to the spatial explanation, because Tie2–angiopoietin signaling occurs between the endothelium and pericytes and thus outside the vessel lumen, the Fc chimera, which is of fairly large molecular size and may therefore be retained inside vessel lumens, is not able to affect signaling. The other drugs used in the present study were all SMWI, which may easily exit the vessel lumen and penetrate the perivascular tissues. The second explanation is temporal. Although this signaling pathway is known to be deeply involved in development, whether it is also involved in the maintenance of endothelial-mural structure is not known. Because we observed the effects of drugs only at 24 h after administration, it is possible that other inhibitors inhibited only the maintenance functions of the signaling pathways, and not functions related to development. Administration of TGF-β inhibitor did not significantly affect the vasculature in normal organs,[7] so it is possible that the neovasculature requires larger amounts of signaling molecules to maintain structure than do established vessels.

In conclusion, the appropriate strategy for optimization of tumor vasculature for drug delivery system using nanoparticles may not be uniform, and may depend on tumor type, including differences in the degree of pericyte coverage of tumor vasculature.

Acknowledgments

We thank Dr Peter Baluk, Cardiovascular Research Institute, University of California, San Francisco (UCSF), for advice about perfusion. This work was supported by Grant-in-Aid for Scientific Research (KAKENHI 19790282 and 17016011) from the Ministry of Education, Culture, Sports, and Technology of Japan (MEXT), and a Health Labor Sciences Research Grant from the Ministry of Health, Labor, and Welfare of Japan.

References

1 Giroux V, Malicet C, Barthet M *et al.* p8 is a new target of gemcitabine in pancreatic cancer cells. *Clin Cancer Res* 2006; **12**: 235–41.
2 Merriman RL, Hertel LW, Schultz RM *et al.* Comparison of the antitumor activity of gemcitabine and ara-C in a panel of human breast, colon, lung and pancreatic xenograft models. *Invest New Drugs* 1996; **14**: 243–7.
3 Rothenberg ML, Moore MJ, Cripps MC *et al.* A phase II trial of gemcitabine in patients with 5-FU-refractory pancreas cancer. *Ann Oncol* 1996; **7**: 347–53.
4 Hanahan D, Weinberg RA. The hallmarks of cancer. *Cell* 2000; **100**: 57–70.
5 Jain RK. Physiological barriers to delivery of monoclonal antibodies and other macromolecules in tumors. *Cancer Res* 1990; **50**: 814S–19S.
6 Dreher MR, Liu W, Michelich CR, Dewhirst MW, Yuan F, Chilkoti A. Tumor vascular permeability, accumulation, and penetration of macromolecular drug carriers. *J Natl Cancer Inst* 2006; **98**: 335–44.
7 Kano MR, Bae Y, Iwata C *et al.* Improvement of cancer-targeting therapy, using nanocarriers for intractable solid tumors by inhibition of TGF-β signaling. *Proc Natl Acad Sci USA* 2007; **104**: 3460–5.
8 Jain RK. Normalization of tumor vasculature: an emerging concept in antiangiogenic therapy. *Science* 2005; **307**: 58–62.
9 Wilhelm S, Carter C, Lynch M *et al.* Discovery and development of sorafenib: a multikinase inhibitor for treating cancer. *Nat Rev Drug Discov* 2006; **5**: 835–44.
10 Bergers G, Song S. The role of pericytes in blood-vessel formation and maintenance. *Neuro Oncol* 2005; **7**: 452–64.
11 von Tell D, Armulik A, Betsholtz C. Pericytes and vascular stability. *Exp Cell Res* 2006; **312**: 623–9.
12 Abramsson A, Lindblom P, Betsholtz C. Endothelial and nonendothelial sources of PDGF-B regulate pericyte recruitment and influence vascular pattern formation in tumors. *J Clin Invest* 2003; **112**: 1142–51.
13 Lindblom P, Gerhardt H, Liebner S *et al.* Endothelial PDGF-B retention is required for proper investment of pericytes in the microvessel wall. *Genes Dev* 2003; **17**: 1835–40.
14 Buchdunger E, Zimmermann J, Mett H *et al.* Inhibition of the Abl protein-tyrosine kinase *in vitro* and *in vivo* by a 2-phenylaminopyrimidine derivative. *Cancer Res* 1996; **56**: 100–4.
15 Bergers G, Song S, Meyer-Morse N, Bergsland E, Hanahan D. Benefits of targeting both pericytes and endothelial cells in the tumor vasculature with kinase inhibitors. *J Clin Invest* 2003; **111**: 1287–95.
16 Kano MR, Morishita Y, Iwata C *et al.* VEGF-A and FGF-2 synergistically promote neoangiogenesis through enhancement of endogenous PDGF-B–PDGFRβ signaling. *J Cell Sci* 2005; **118**: 3759–68.
17 Vlahovic G, Rabbani ZN, Herndon JE, Dewhirst MW, Vujaskovic Z. Treatment with Imatinib in NSCLC is associated with decrease of phosphorylated PDGFR-β and VEGF expression, decrease in interstitial fluid pressure and improvement of oxygenation. *Br J Cancer* 2006; **95**: 1013–19.
18 Mancuso MR, Davis R, Norberg SM *et al.* Rapid vascular regrowth in tumors after reversal of VEGF inhibition. *J Clin Invest* 2006; **116**: 2610–21.
19 Hurwitz H, Fehrenbacher L, Novotny W *et al.* Bevacizumab plus irinotecan, fluorouracil, and leucovorin for metastatic colorectal cancer. *N Engl J Med* 2004; **350**: 2335–42.
20 Hirschi KK, Rohovsky SA, D'Amore PA. PDGF, TGF-β, and heterotypic cell–cell interactions mediate endothelial cell-induced recruitment of 10T1/2 cells and their differentiation to a smooth muscle fate. *J Cell Biol* 1998; **141**: 805–14.
21 Pietras K, Pahler J, Bergers G, Hanahan D. Functions of paracrine PDGF signaling in the proangiogenic tumor stroma revealed by pharmacological targeting. *PLoS Med* 2008; **5**: e19.
22 Micke P, Ostman A. Tumour-stroma interaction: cancer-associated fibroblasts as novel targets in anti-cancer therapy? *Lung Cancer* 2004; **45**: S163–75.
23 Bhowmick NA, Moses HL. Tumor–stroma interactions. *Curr Opin Genet Dev* 2005; **15**: 97–101.
24 Lewis CE, Pollard JW. Distinct role of macrophages in different tumor microenvironments. *Cancer Res* 2006; **66**: 605–12.
25 Armulik A, Abramsson A, Betsholtz C. Endothelial/pericyte interactions. *Circ Res* 2005; **97**: 512–23.

doi: 10.1111/j.1349-7006.2008.01003.x

Diffuse-Type Gastric Carcinoma: Progression, Angiogenesis, and Transforming Growth Factor β Signaling

Akiyoshi Komuro, Masakazu Yashiro, Caname Iwata, Yasuyuki Morishita, Erik Johansson, Yoshiko Matsumoto, Akira Watanabe, Hiroyuki Aburatani, Hiroyuki Miyoshi, Kunihiko Kiyono, Yo-taro Shirai, Hiroshi I. Suzuki, Kosei Hirakawa, Mitsunobu R. Kano, Kohei Miyazono

Background Diffuse-type gastric carcinoma is a cancer with poor prognosis that has high levels of transforming growth factor β (TGF-β) expression and thick stromal fibrosis. However, the association of TGF-β signaling with diffuse-type gastric carcinoma has not been investigated in detail.

Methods We used a lentiviral infection system to express a dominant-negative TGF-β type II receptor (dnTβRII) or green fluorescent protein (GFP) as a control in the diffuse-type gastric carcinoma cell lines, OCUM-2MLN and OCUM-12. These infected cells and the corresponding parental control cells were subcutaneously or orthotopically injected into nude mice. Angiogenesis was inhibited by infecting cells with a lentivirus carrying the gene for angiogenic inhibitor thrombospondin-1 or by injecting mice intraperitoneally with the small-molecule angiogenic inhibitor sorafenib or with anti-vascular endothelial growth factor (VEGF) neutralizing antibody (six or eight mice per group). Expression of phospho-Smad2 and thrombospondin-1 was investigated immunologically in human gastric carcinoma tissues from 102 patients. All statistical tests were two-sided.

Results Expression of dnTβRII into OCUM-2MLN cells did not affect their proliferation in vitro, but it accelerated the growth of subcutaneously or orthotopically transplanted tumors in vivo (eg, for mean volume of subcutaneous tumors on day 10 relative to that on day 0: dnTβRII tumors = 3.49 and GFP tumors = 2.46, difference = 1.02, 95% confidence interval [CI] = 0.21 to 1.84; $P = .003$). The tumors expressing dnTβRII had higher levels of angiogenesis than those expressing GFP because of decreased thrombospondin-1 production. Similar results were obtained with OCUM-12 cells. Expression of thrombospondin-1 in the dnTβRII tumor or treatment with sorafenib or anti-VEGF antibody reduced tumor growth, whereas knockdown of thrombospondin-1 expression resulted in more accelerated growth of OCUM-2MLN tumors than of GFP tumors (eg, mean tumor volumes on day 14 relative to those on day 0: thrombospondin-1–knockdown tumors = 4.91 and GFP tumors = 3.79, difference = 1.12, 95% CI = 0.80 to 1.44; $P < .001$). Positive association between phosphorylated Smad2 and thrombospondin-1 immunostaining was observed in human gastric carcinoma tissues.

Conclusions Disruption of TGF-β signaling in diffuse-type gastric carcinoma models appeared to accelerate tumor growth, apparently through increased tumor angiogenesis that was induced by decreased expression of thrombospondin-1.

J Natl Cancer Inst 2009;101:592–604

Gastric cancer is one of the most devastating human cancers, with approximately 880000 new cases and 650000 deaths worldwide per year (1,2). There are two types of gastric cancer: diffuse type and intestinal type. Diffuse-type gastric carcinoma, according to the Laurén classification (3), is highly metastatic and characterized clinically by rapid disease progression and poor prognosis (4). Although the incidence of intestinal-type gastric carcinoma has continuously decreased, the incidence of diffuse-type gastric carcinoma has increased progressively during the last 30 years, so that

Affiliations of authors: Department of Molecular Pathology and the Global Center of Excellence Program for "Integrative Life Science Based on the Study of Biosignaling Mechanisms," Graduate School of Medicine (AK, CI, YMo, EJ, YMa, KK, Y-tS, HIS, MRK, KM), Center for NanoBio Integration (MRK, KM), and Genome Science Division, Research Center for Advanced Science and Technology (AW, HA), University of Tokyo, Tokyo, Japan; Department of Surgical Oncology, Osaka City University Graduate School of Medicine, Osaka, Japan (MY, KH); Subteam for Manipulation of Cell Fate, Bio Resource Center, RIKEN, Tsukuba, Japan (HM).

Correspondence to: Kohei Miyazono, MD, Department of Molecular Pathology, Graduate School of Medicine, University of Tokyo, Hongo 7-3-1, Bunkyo-ku, Tokyo 113-0033, Japan (e-mail: miyazono-ind@umin.ac.jp).

See "Funding" and "Notes" following "References."

DOI: 10.1093/jnci/djp058

the diffuse type constitutes approximately one-third of all gastric carcinomas diagnosed in the United States (5). In contrast to the intestinal type, infection with *Helicobacter pylori* and chronic gastritis are often absent in the diffuse-type gastric carcinoma. Patients with diffuse-type gastric carcinoma often have thick stromal fibrosis with undifferentiated carcinoma cells scattered in the interstitium, which results in a stiff and thick gastric wall with reduced motility, but the tumors do not form ulcers or apparent mass lesions.

Transforming growth factor β (TGF-β) is a multifunctional cytokine that contributes to cancer progression by acting in both tumor cells and the tumor stroma (6). TGF-β binds to TGF-β serine–threonine kinase receptors type I and type II (TβRII) and transduces signals by phosphorylation of the receptor-regulated Smad2 and Smad3 proteins. Smad2 and Smad3 form complexes with Smad4, and these complexes regulate transcription of various target genes in the nucleus (7,8).

Because TGF-β is a potent inhibitor of epithelial cell proliferation, resistance to the inhibitory activity of TGF-β results in increased cell proliferation and cancer progression (9). Cancer cells in advanced tumors are often refractory to TGF-β–induced growth inhibition, and some tumors even increase their production of TGF-β ligands. TGF-β induces deposition of extracellular matrix in the tumor interstitium, which leads to fibrosis. TGF-β also induces perturbations of immune surveillance and regulates angiogenesis in vivo. Moreover, TGF-β may promote tumor growth by inducing epithelial cells to undergo the epithelial–mesenchymal transition (10,11), and inhibition of TGF-β signaling has been reported to prevent progression and metastasis of certain advanced tumors (12–15). In addition, decreased expression of TβRII, Smad2, and/or Smad4 or loss-of-function mutations in at least one of these genes has been observed in advanced stages of certain cancers, including colorectal cancer, breast cancer, and prostate cancer (16), and these changes in TGF-β signaling may affect progression of these cancers.

There is limited information regarding the role of TGF-β in diffuse-type gastric cancers. The thick stromal fibrosis observed in diffuse-type gastric carcinoma is induced by the TGF-β produced by cancer cells and by cancer-associated fibroblasts (17). Production of TGF-β1 has been reported to be associated with the progression of diffuse-type gastric carcinoma (18), although the relation of TGF-β1 expression to prognosis of gastric carcinoma is controversial (19). Disruption of TGF-β signaling by loss of Smad4 expression has also been observed in diffuse-type gastric carcinoma (20). However, detailed investigations on the roles of TGF-β signaling in diffuse-type gastric carcinoma have not been carried out. We therefore investigated the role of TGF-β signaling in diffuse-type gastric carcinoma by use of OCUM-2MLN and OCUM-12 cell lines and by disrupting TGF-β signaling.

CONTEXT AND CAVEATS

Prior knowledge

Diffuse-type gastric carcinoma has poor prognosis. Patients have high levels of transforming growth factor β (TGF-β) expression and thick stromal fibrosis.

Study design

The roles of TGF-β and thrombospondin-1, an angiogenic inhibitor that is regulated by TGF-β, were investigated in vitro studies in diffuse-type gastric carcinoma cell lines and in vivo studies in mouse models of diffuse-type gastric carcinoma and human diffuse-type gastric carcinoma tissue specimens from 102 patients.

Contribution

Growth of diffuse-type gastric carcinomas appeared to be accelerated by disruption of TGF-β signaling in mouse models (which may be analogous to what occurs during progression of this disease in humans), apparently because of increased tumor angiogenesis that was induced by decreased expression of thrombospondin-1.

Implications

Because loss of a receptor for TGF-β has been reported to induce tumor angiogenesis in various cancers, administration of angiogenesis inhibitors, such as sorafenib or thrombospondin-1 analogues, should be investigated as a treatment for cancers with disrupted TGF-β signaling pathways.

Limitations

Although mouse models of subcutaneous and orthotopic transplantation models were used, the experiments were conducted with immunocompromised mice. The growth of metastatic tumors was not investigated.

From the Editors

Patients, Materials, and Methods

Cell Lines

The OCUM-2MLN cell line was obtained from a lymph node metastasis of a mouse with orthotopically implantated OCUM-2M cells (21); the OCUM-2M line was originally established from a 49-year-old woman with diffuse-type gastric carcinoma (4). The OCUM-12 cell line was established from the peritoneal effusion of a 58-year-old man with diffuse-type gastric carcinoma that was diagnosed by endoscopy and histology. OCUM-12 cells were further confirmed to be tumorigenic in nude mice [(22) and M. Yashiro and K. Hirakawa, Osaka City University, unpublished data]. Both cell lines were cultured in Dulbecco's modified Eagle medium (DMEM) containing 10% fetal bovine serum, penicillin (100 U/mL), and streptomycin (0.1 mg/mL) (Invitrogen, Carlsbad, CA). To disrupt TGF-β signaling, we introduced a dominant-negative TGF-β type II receptor (dnTβRII) that lacks the intracellular kinase domain into the OCUM-2MLN and OCUM-12 cell lines (resulting in the 2MLN-dnTβRII and OCUM-12-dnTβRII cell lines, respectively) by use of a lentiviral infection system (23). We used the same lentivirus system to generate control OCUM-2MLN and OCUM-12 cells that expressed green fluorescent protein (GFP) (resulting in the 2MLN-GFP and OCUM-12-GFP cell lines, respectively) and OCUM-2MLN cells that expressed both dnTβRII and the angiogenic inhibitor thrombospondin-1 (resulting in the 2MLN-dnTβRII+TSP-1) (24,25). cDNAs for dnTβRII or for thrombospondin-1 were produced from mRNA extracted from the cultured OCUM-2MLN cell line by polymerase chain reaction (PCR). cDNAs encoding either dnTβRII with a carboxyl-terminal hemagglutinin epitope tag or thrombospondin-1 were inserted into the multicloning site of the lentiviral

vector pCSII-CMV-RfA by use of pENTR, according to the manufacturer's protocol (Invitrogen).

Antibodies and Reagents

The rabbit polyclonal antibodies against human and mouse phosphorylated Smad2 that were used for immunoblotting were a gift from A. Moustakas and C.-H. Heldin (Ludwig Institute for Cancer Research, Uppsala, Sweden). The rabbit monoclonal antibody against human and mouse phosphorylated Smad2 that was used for immunohistochemistry was from Millipore (Temecula, CA; clone A5S). The rat monoclonal antibody against mouse platelet–endothelial cell adhesion molecule-1 (PECAM-1) and mouse monoclonal antibody against human and mouse Smad2 and Smad3 (clone 18) were from BD (Franklin Lakes, NJ). The rat monoclonal antibody against hemagglutinin tag (clone 3F10) was from Roche (Basel, Swiss), and mouse monoclonal antibody against GFP (clone 1E4) was from Medical & Biological Laboratories, Co. (Woburn, MA). Mouse monoclonal antibody against human and mouse thrombospondin-1 was from Abcam (Cambridge, UK; clone A6.1). Alexa 488– and Alexa 594–conjugated secondary antibodies and the nuclear stain TOTO-3 for counterstaining were from Invitrogen Molecular Probes (Eugene, OR). TGF-β3 and TGF-β1, which show similar biological activities in vitro, were purchased from R&D Systems (Minneapolis, MN).

Immunoblot Analysis

We examined the expression of Smad2 and Smad3, phosphorylated Smad2, GFP, and hemagglutinin-tagged dnTβRII by immunoblot analyses in following cultured cells: 2MLN, 2MLN-GFP, 2MLN-dnTβRII, OCUM-12, OCUM-12-GFP, and OCUM-12-dnTβRII. These cells were lysed in a buffer containing 50 mM Tris–HCl (pH 8.0), 150 mM NaCl, 1% Nonidet P-40 (Nacalai Tesque, Kyoto, Japan), 5 mM EDTA, 0.5% deoxycholic acid sodium salt-monohydrate (Nacalai Tesque), 0.1% sodium dodecyl sulfate (SDS) (Nacalai Tesque), 1% aprotinin (Mitsubishi Pharma, Osaka, Japan), and 1 mM phenylmethylsulfonyl fluoride (Sigma, St Louis, MO). The cell lysates were boiled in SDS sample buffer (100 mM Tris–HCl at pH 8.8, 0.01% bromophenol blue, 36% glycerol, 4% SDS, and 10 mM dithiothreitol) and subjected to SDS–polyacrylamide gel electrophoresis. Proteins were electrotransferred from a polyacrylamide gel to Pall Fluorotrans-W membranes (Pall, East Hills, NY) and immunoblotted with antibodies. Bound antibodies were detected by use of an enhanced chemiluminescence detection system (Amersham Pharmacia Biotech, Piscataway, NJ). Each experiment was conducted two times, and a representative result is shown.

Cell Proliferation Assay

We cultured 2.5×10^4 2MLN, 2MLN-GFP, 2MLN-dnTβRII, or OCUM-12 cells per well in 12-well plates. On the next day (designated as day 0), some cultures were treated with TGF-β and control cultures were left untreated. Cells from duplicate cultures were counted as indicated with a hemocytometer. Each experiment was conducted two times, sample points were assayed in triplicate, and data were averaged. Data from one representative experiment of these are shown.

BALB/c Nude Mouse Model for Human Gastric Cancer

BALB/c nude male mice, aged 4–5 weeks, were obtained from Oriental Yeast Co. (Tokyo, Japan). All animal experimental protocols were performed in accordance with the policies of the Animal Ethics Committee of the University of Tokyo. A total of 5×10^6 cells in 100 μL of DMEM ($n > 6$ mice per group) was injected subcutaneously at the left flank of each mouse and allowed to grow for 1 week (for OCUM-2MLN cells) or 3 weeks (for OCUM-12 cells) when the major axis of the tumors was approximately 10 mm long. For the orthotopic transplantation model, a total of 5×10^6 cells in 50 μL of DMEM were injected into the gastric wall of each mouse ($n = 8$ mice per group) and allowed to grow for 1 week when tumor was approximately 5 mm in diameter.

Tumor Volume Measurement

The volume of subcutaneous xenograft tumors was measured externally every other day until the end of the evaluation period. Tumor volume was estimated by using the equation, $v = (ab^2)/2$, where v is volume, a is the length of the major axis of the tumor, and b is the length of its minor axis. The relative tumor volume was then calculated by dividing tumor volume on a given experimental day by that on day 0 (the day of initiation of treatment or evaluation). For orthotopic xenograft tumors, the tumor area on the gastric wall was measured by opening the abdomen on experimental day 14 and at the end of the evaluation period (day 21). The major and minor axes of tumors were measured with Adobe Photoshop software (Adobe Systems, Mountain View, CA), and tumor areas on the gastric wall were calculated with ImageJ software (National Institutes of Health, Bethesda, MD). Relative tumor area was obtained by dividing the area on day 21 by that on day 14.

RNA Isolation and Quantitative Real-Time Reverse Transcription-PCR

Total RNAs from gastric carcinoma cells or excised subcutaneous tumors were extracted with the RNeasy Mini Kit (QIAGEN, Valencia, CA). Sources of RNAs were as follows: cultured 2MLN, 2MLN-GFP, and 2MLN-dnTβRII cells at 0, 1, and 24 hours treated with TGF-β ligand at 1 ng/mL or left untreated (*see* Figure 1, B); cultured 2MLN-GFP and 2MLN-dnTβRII cells at 24 hours treated with TGF-β ligand at 1 ng/mL or left untreated, and subcutaneous tumors generated from these cells that were allowed to grow for 3 weeks in vivo (*see* Figure 2); cultured 2MLN-GFP, 2MLN-GFP+miTSP-1, and 2MLN-dnTβRII cells treated with TGF-β ligand at 1 ng/mL or left untreated, and subcutaneous tumors generated from these cells in vivo that were allowed to grow for 3 weeks (*see* Figure 4); and cultured OCUM-12-GFP and OCUM-12-dnTβRII cells at 24 hours treated with TGF-β ligand at 1 ng/mL or left untreated (*see* Figure 5). First-strand cDNAs were synthesized with the Quantitect Reverse Transcription kit (QIAGEN) with random hexamer primers. Quantitative real-time reverse transcription (RT)-PCR analysis was performed with the 7500 Fast Real-Time PCR system (Applied Biosystems, Foster City, CA) with the primers, as shown in Supplementary Table 1 (available online). Each experiment was conducted two times, each sample was assayed in triplicate, and data were averaged. Data from one representative experiment are shown.

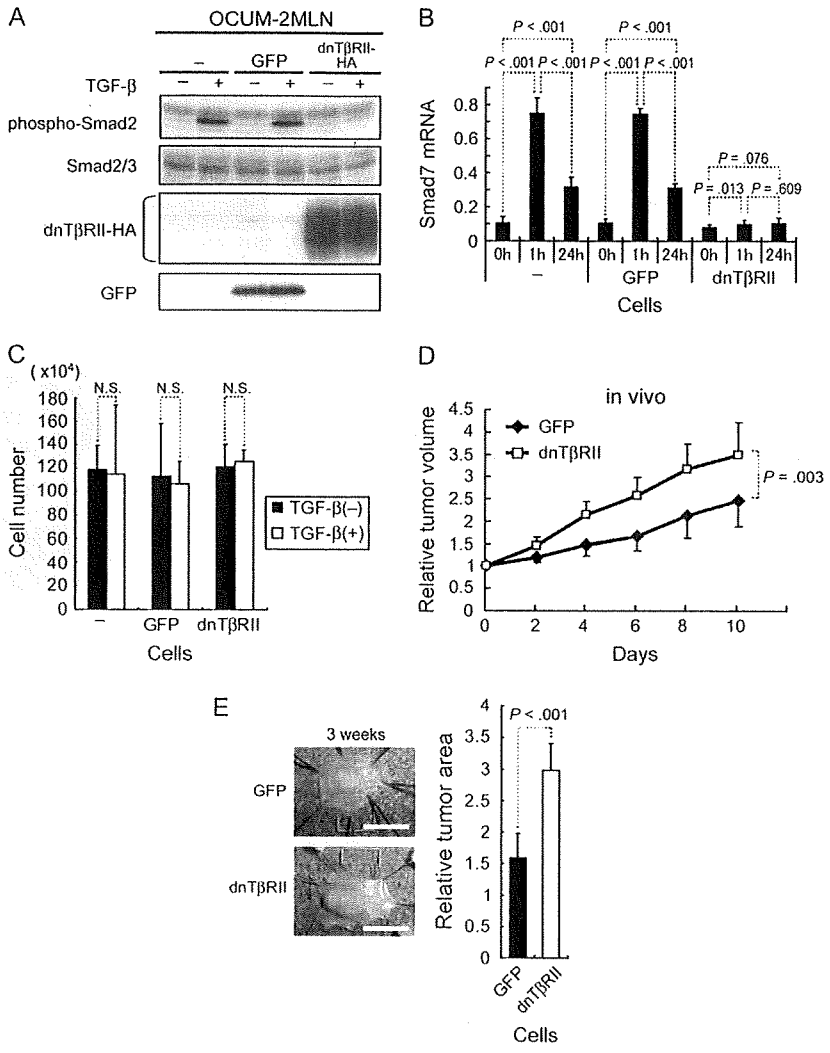

Figure 1. Disruption of TGF-β in gastric cancer cells and tumors. We used parental OCUM-2MLN cells, 2MLN cells expressing GFP (termed 2MLN-GFP cells) as a control, and 2MLN cells expressing a dnTβRII (termed 2MLN-dnTβRII cells). **A)** TGF-β signal transduction in the cells. Immunoblot analysis was used to compare the level of phosphorylated Smad2 (phospho-Smad2) with that of Smad2 and 3 as control, in parental OCUM-2MLN cells (**lanes** – = cells carry no constructs), 2MLN-GFP cells (**lanes GFP**), and 2MLN-dnTβRII cells (**lanes dnTβRII**), treated with TGF-β3 (1 ng/mL) or left untreated for 1 hour. Expression of dnTβRII protein (by use of hemagglutinin [HA] tag), and that of GFP, as a control for lentiviral infection was also determined by immunoblot analysis. The cells were subjected to immunoblot analysis with antibodies against the proteins indicated to the **left**. The experiment was conducted two times, and data from one representative experiment are shown. **B)** Human Smad7 mRNA expression. Quantitative real-time polymerase chain reaction was used to assess the level of expression of human Smad7 mRNA in all three cell lines after treatment with TGF-β3 (1 ng/mL), as indicated. The experiment was conducted two times, each sample was assessed in triplicate, and data were averaged. Data from one representative experiment are shown. **C)** Proliferation of gastric cancer cells in the presence of TGF-β3. Cells were treated with TGF-β3 (1 ng/mL) in 10% fetal bovine serum for 3 days; control cells were not treated with TGF-β3. The experiment was conducted two times, each sample was assessed in triplicate, and data were averaged. Data from one representative experiment are shown. **D)** Growth of 2MLN-GFP and 2MLN-dnTβRII tumors in nude mice for 10 days. Cells were subcutaneously transplanted into nude mice (n = 8 mice per group). **E)** Growth of orthotopic 2MLN-GFP and 2MLN-dnTβRII tumors in nude mice. Cells were transplanted into the gastric wall of nude mice (n = 8 mice per group). **Left)** Macroscopic appearance of representative samples of excised gastric wall with an orthotopic tumor. **Right)** Relative areas of the 2MLN-GFP and 2MLN-dnTβRII tumors. Scale bar = 10 mm. **Error bars** = 95% confidence intervals. All *P* values (two-sided) were calculated by using a Student's *t* test, except for that in **(D)**, which was calculated by using a two-way repeated measures analysis of variance. dnTβRII = dominant-negative TGF-β type II receptor; GFP = green fluorescent protein; TGF-β = transforming growth factor β.

Microarray Analysis of Gene Expression in 2MLN-GFP or 2MLN-dnTβRII Tumors

Tissue samples from subcutaneous 2MLN-GFP or 2MLN-dnTβRII tumors were digested with collagenase (Worthington, Lakewood, NJ; 1 mg/mL) at 37°C for 1 hour, followed by treatment with 0.25% trypsin–EDTA (Invitrogen) at 37°C for 15 minutes. The resulting single-cell suspension was subjected to magnetic cell sorting (MACS®) with magnetic microbeads conjugated to CD326 antibody (Miltenyi Biotec, Auburn, CA) to separate CD326-positive human cancer cells from CD326-negative mouse stromal cells. Total RNAs from the isolated cancer cells were purified with the RNeasy Mini Kit (QIAGEN) and used for microarray analysis. Biotin-labeled complementary RNAs were synthesized and hybridized to the oligonucleotide microarray, GeneChip Human Genome U133 Plus2.0 (Affymetrix, Santa Clara, CA), according to Affymetrix technical manual. Gene expression data were normalized by use of the MAS5 algorithm according to the manufacturer's instruction. DAVID functional annotation clustering (26) with the Kyoto Encyclopedia of Genes and Genomes pathway database (http://genome.ad.jp/kegg/) was used for pathway analysis of the top 50 most variable probe sets of the GeneChip.

Histochemistry and Immunohistochemistry in Mouse Tissues

Excised mouse tissue samples were fixed for 1 hour in 10% neutral-buffered formalin at room temperature, washed overnight in phosphate-buffered saline containing 10% sucrose at 4°C, and embedded in optimal cutting temperature compound (Tissue-Tek; Sakura Finetek, Tokyo, Japan). Some samples were then snap frozen in a dry ice–acetone bath for immunohistochemistry, and other samples were fixed overnight in 4% paraformaldehyde and then embedded in paraffin for hematoxylin–eosin staining or AZAN staining to visualize collagen fibers. Frozen samples were

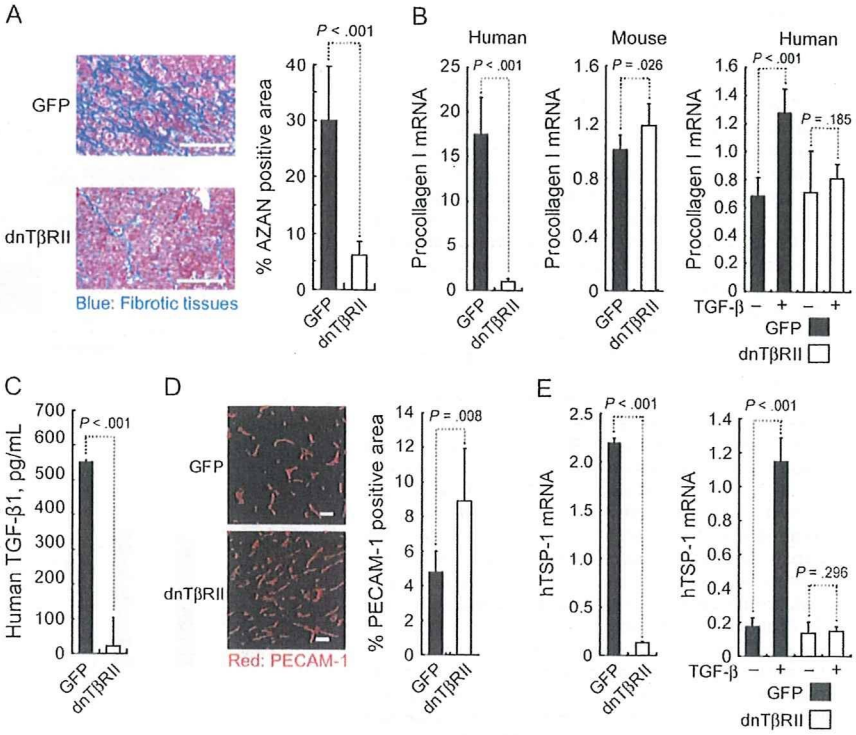

Figure 2. Histological characterization of 2MLN-GFP and 2MLN-dnTβRII xenograft tumors from nude mice. **A)** Fibrotic tissue in subcutaneous 2MLN-GFP (GFP) or 2MLN-dnTβRII (dnTβRII) xenograft tumors. **Left)** On day 14, fibrotic areas of tumor sections were visualized by AZAN staining and examined via light microscopy. Scale bars = 100 μm. **Right)** Quantification of fibrotic areas (n = 9 with each condition). **B)** Expression of human and mouse procollagen I mRNAs. **Left)** 2MLN-GFP subcutaneous tumors in nude mice. **Middle)** 2MLN-dnTβRII subcutaneous tumors in nude mice. **Right)** TGF-β treatment in 2MLN-GFP and 2MLN-dnTβRII cell lines. Cells were treated with TGF-β for 24 hours or left untreated (as indicated) and assayed for procollagen I mRNA with quantitative real-time polymerase chain reaction. Each experiment was conducted two times, each sample was assessed in triplicate, and data were averaged. Data from one representative experiment of these are shown. **C)** Concentrations of human TGF-β1 protein in 2MLN-GFP and 2MLN-dnTβRII cell culture supernatants. The level of TGF-β1 protein was determined by an enzyme-linked immunosorbent assay with an antibody specific for TGF-β1. The experiment was conducted two times, each sample was assessed in triplicate, and data were averaged. Data from one representative experiment of these are shown. **D)** Vascular density in 2MLN-GFP and 2MLN-dnTβRII xenograft tumors. Vascular density was determined by immunostaining with an antibody against PECAM-1 (n = 6 mice per group). **Left)** Micrographs of immunostained 2MLN-GFP and 2MLN-dnTβRII xenograft tumor sections. PECAM-1–positive areas are shown in **red** (n = 6 with each condition). Scale bars = 100 μm. **Right)** Percent PECAM-1–positive areas in 2MLN-GFP and 2MLN-dnTβRII xenograft tumor sections per microscopic field (n = 6 with each condition). **E)** Expression of hTSP-1 mRNA. **Left)** 2MLN-GFP and 2MLN-dnTβRII tumors in nude mice. **Right)** 2MLN-GFP and 2MLN-dnTβRII cells treated with TGF-β or left untreated for 24 hours in vitro, as indicated. Each experiment was conducted two times, each sample was assessed in triplicate, and data were averaged. Data from one representative experiment are shown. **Error bars** = 95% confidence intervals. All *P* values (two-sided) were calculated with a Student's *t* test. dnTβRII = dominant-negative TGF-β type II receptor; GFP = green fluorescent protein; TGF-β = transforming growth factor β; hTSP-1 = human thrombospondin-1; PECAM-1 = platelet–endothelial cell adhesion molecule-1.

further sectioned at a thickness of 10 μm with a cryostat, briefly fixed with 10% formalin, and then incubated with primary and secondary antibodies. Formalin-fixed samples of subcutaneous tumors and orthotopic tumors were subjected to hematoxylin–eosin and AZAN staining (*see* Figures 2, A and 4, C and Supplementary Figure 1, A, available online). Frozen samples of subcutaneous tumors were immunostained with anti-PECAM-1 and anti-rat Alexa 594 antibodies (*see* Figures 2, D and 4, B), or with anti-hemagglutinin and anti-rat Alexa 594 antibodies with TOTO-3 nuclear stain (*see* Figure 3, B). Frozen samples of orthotopic tumors were immunostained with anti-PECAM-1 and anti-rat Alexa 594 antibody (Supplementary Figure 1, B, available online).

Enzyme-Linked Immunosorbent Assay

Production of TGF-β1 by 2MLN-GFP and 2MLN-dnTβRII cells was determined with a sandwich enzyme immunoassay technique by using a Quantikine human TGF-β1 immunoassay (R&D Systems), according to the manufacturer's instruction. A total of 1×10^6 cells were cultured in 1% fetal bovine serum in six-well plates for 24 hours, and 100 μL of conditioned medium was removed and treated with 20 μL of 1 M HCl for 10 minutes, followed by neutralization with 20 μL of 1.2 M NaOH in 0.5 M HEPES (pH 7.4). Without this acidification step with 1 M HCl, levels of TGF-β1 in the conditioned medium could not be detected by the enzyme-linked immunosorbent assay. The samples were then pipetted into the wells of the microplate that had been precoated with a monoclonal antibody specific for TGF-β1 and incubated for 2 hours at room temperature. Subsequently, an enzyme-linked polyclonal antibody specific for TGF-β1 was added to the wells and incubated for additional 2 hours at room temperature to sandwich the TGF-β1 ligand. After a wash to remove unbound antibody–enzyme reagent, a substrate solution consisting of hydrogen peroxide and tetramethylbenzidine was added to the wells, and the intensity of the color developed was determined with a microplate reader (BIO-RAD, Hercules, CA). Each experiment was conducted two times, each sample point was assessed in triplicate, and data were averaged. Data from one representative experiment are shown.

Reduction of Thrombospondin-1 Expression by Use of MicroRNAs

The Block-iT Pol II miR RNAi expression system (Invitrogen) was used to knockdown the expression of thrombospondin-1. A microRNA construct against thrombospondin-1 was cloned into the pcDNA6.2-GW/EmGFP-mir vector (Invitrogen) after annealing the oligonucleotide 5′-AGAACTCAGTTACCATCTGCA-3′, which was designed to knockdown the expression of thrombospondin-1 by using BLOCK-iT RNAi Designer (Invitrogen). The EmGFP-miR thrombospondin-1 expression site was then inserted

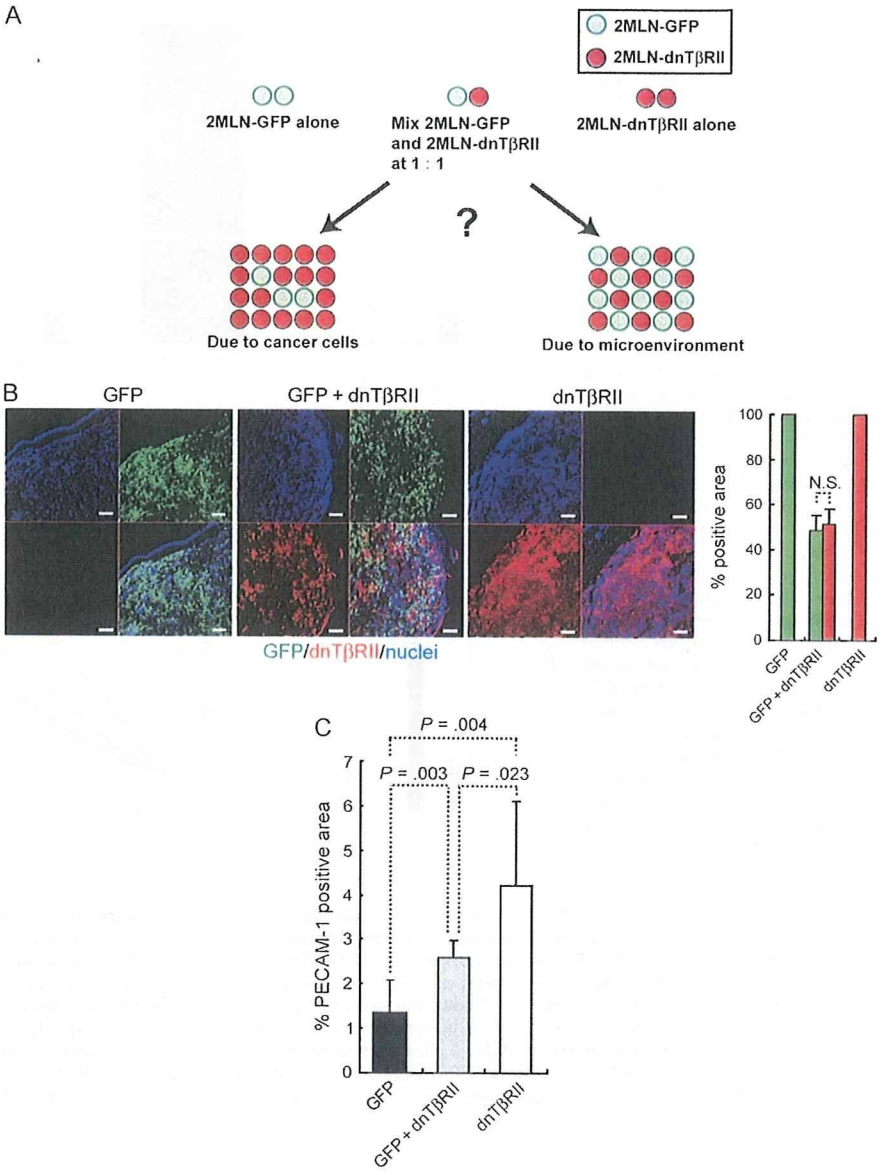

Figure 3. Characterization of xenograft tumors with a mixture of equal numbers of 2MLN-GFP (GFP) and 2MLN-dnTβRII (dnTβRII) cells. **A)** Developmental model of tumors inoculated with a mixture of 2MLN-GFP and 2MLN-dnTβRII. Equal amounts of the 2MLN-GFP and 2MLN-dnTβRII cells were mixed and transplanted into nude mice. The composition of tumors generated with a mixture of 2MLN-GFP and 2MLN-dnTβRII cells was compared with that of tumors generated with 2MLN-GFP or 2MLN-dnTβRII cells alone to investigate whether the tumor microenvironment serves as a major determinant of tumor growth. **B)** Distribution of 2MLN-GFP cells (GFP, **green**) and 2MLN-dnTβRII cells (as shown by a hemagglutinin tag that was detected with anti-hemagglutinin antibody, **red**) in mixed-cell tumors. 2MLN-GFP cells were identified by GFP fluorescence, and 2MLN-dnTβRII cells were identified by immunohistochemistry staining with an antibody specific for hemagglutinin and with nuclear counterstaining with TOTO-3. **Left)** Micrographs of sections from tumors generated with 2MLN-GFP cells alone, 2MLN-dnTβRII cells alone, or a mixture of both cell lines. Scale bars = 100 μm. **Right)** Percent hemagglutinin-positive areas and GFP-positive areas (n = 9 with each condition). **C)** Vascular areas in tumors generated with 2MLN-GFP cells alone, 2MLN-dnTβRII cells alone, or a mixture of both cell types. Vascular areas were identified by immunostaining with antibody against PECAM-1 (n = 3 in each condition). **Error bars** = 95% confidence intervals. All *P* values (two-sided) were calculated using the Student's *t* test. dnTβRII = dominant-negative TGF-β type II receptor; GFP = green fluorescent protein; TGF-β = transforming growth factor β; PECAM-1 = platelet–endothelial cell adhesion molecule-1.

into the pDONR221 vector (Invitrogen) by the BP recombination reaction according to the manufacturer's instructions, followed by its insertion into multicloning site of the lentiviral vector pCSII-EF-MCS LR recombination reaction (Invitrogen), according to the manufacturer's instruction. Stably transfected 2MLN-GFP cells, termed 2MLN-GFP+miTSP-1, in which the expression of thrombospondin-1 was silenced, were established by use of the lentiviral infection system by the methods as described above (23).

Treatment With Angiogenesis Inhibitors In Vivo

A small-molecule inhibitor of angiogenesis, sorafenib (Nexavar; Bayer Health Care, Leverkusen, Germany), was dissolved at 10 mg/mL in dimethyl sulfoxide as stock solution (ie, 5 mL of dimethyl sulfoxide was added to one-fourth of a 200-mg sorafenib tablet). An 80-μL aliquot of the sorafenib stock solution (800 μg of sorafenib) was diluted with 170 μL of phosphate-buffered saline to a final concentration of 3.2 mg/mL. One week after subcutaneous transplantation with 2MLN-GFP or 2MLN-dnTβRII cells or 4 weeks after subcutaneous transplantation with OCUM-12-GFP and OCUM-12-dnTβRII cells (n = 6 mice per group), sorafenib or a vehicle control was administered intraperitoneally to BALB/c nude mice every day. Fifty micrograms of anti-vascular endothelial growth factor (VEGF) neutralizing monoclonal antibody (MAB293; R&D Systems) (2.5 mg/kg) dissolved in 250 μL of phosphate-buffered saline to a concentration of 0.2 mg/mL or vehicle was intraperitoneally injected into these nude mice (n = 6 mice per group) twice a week for 14 days.

Immunohistochemistry of Human Gastric Cancer Tissues

We examined 102 consecutive surgical samples from patients with gastric cancer at the Osaka City University Hospital, Osaka, Japan,